Ore Geology Reviews 164 (2024) 105829

Contents lists available at ScienceDirect

Ore Geology Reviews

journal homepage: www.elsevier.com/locate/oregeorev

Superimposed multi-stage mineralization in the Qingchengzi Pb-Zn ore district, North China: Evidence from geochronology and sulfide geochemistry

Xiaoxia Duan [a,b,*], Lingli Zhou [c,d], Qingdong Zeng [e,*], Yongbin Wang [f], Zhiqiang Wang [a,b], Bing Yu [g,h]

[a] School of Resources and Environmental Engineering, Hefei University of Technology, Hefei 230009, China
[b] Ore Deposit and Exploration Center (ODEC), Hefei University of Technology, Hefei 230009, China
[c] State Key Laboratory of Ore Deposit Geochemistry, Institute of Geochemistry, Chinese Academy of Sciences, Guiyang 550081, China
[d] Department of Earth Sciences, Vrije Universiteit Amsterdam, De Boelelaan 1105, 1081 HV Amsterdam, Netherlands
[e] Key Laboratory of Mineral Resources, Institute of Geology and Geophysics, Chinese Academy of Sciences, Beijing 100029, China
[f] Yunnan Key Laboratory of Earth System Science, Yunnan University, Kunming 650500, China
[g] Development and Research Centre, China Geological Survey, Beijing 100037, China
[h] Mineral Exploration Technical Guidance Center, Ministry of Natural Resources, Beijing 100037, China

ARTICLE INFO

Keywords:
Pyrite
Sphalerite
In-situ sulfur isotope and trace element
Apatite and zircon geochronology
Multi-stage mineralization
Qingchengzi Pb-Zn ore district

ABSTRACT

The Qingchengzi Pb-Zn polymetallic ore district in northern China records two stages of Pb-Zn mineralization in the Paleoproterozoic and Mesozoic, respectively. The Paleoproterozoic sedimentary-metamorphic stage (stage I) of mineralization was primarily recorded by stratiform ores, and the Mesozoic magmatic-hydrothermal stage (stage II) of mineralization mostly formed vein-type ores. The apatites coexisting with the stage I sulfides yield U-Pb isotopic ages of (1882–1857 Ma), corresponding to the regional metamorphism pervaded in the Paleoproterozoic in the Liaodong region. Zircons from a granite porphyry that is spatially associated with the stage-II mineralization have a U-Pb age of 228.5 ± 5.8 Ma.

Stage-I fine-grained sulfides (Py1a and Sp1a) are of SEDEX origin and the fluid is fertile in metals such as Co, Ni, Zn, As, Mn and V. The metals are likely to be sourced from the Liaohe Group, which contains high concentration of those metals. Stage-I recrystallized sulfides (Py1b and Sp1b) show trace elements such as Co, Ni, Cu, As and Au of pyrite and the Cu, Cd, In, Ag, Sb of sphalerite were remobilized out from their crystal lattice under metamorphism. Stage-II sulfides (Py2 and Sp2) are more enriched in Au, As, Cu, Ag, Sb, Pb compared to stage-I sulfides. LA-ICP-MS mapping reveals multigenerational texture of Py2 which features a Cu and Zn enriched core (Py2a) and an overgrowth rim (Py2b) of enrichment in Au, As, Co and Ni. The compositionally distinct core and rim presumably suggest that two episodes of magmatic fluids are involved in the formation of stage-II sulfides. The sedimentary pyrite from Liaohe Group and the stage-I sulfides have $\delta^{34}S$ value in the ranges of 10.4–17.04 ‰ and 4.10–9.37 ‰, respectively, suggesting that sulfur was probably derived from seawater sulfate reduction. The sulfur isotopes of stage-II sulfides ($\delta^{34}S$ = 4.10–9.02 ‰) reflects a mixing of magmatic sulfur with sulfur leached from *meta*-volcanic-sedimentary source. This process was associated with the upward migration of magmatic hydrothermal fluids and subsequent fluid-rock interaction, which leached heavy sulfur isotopes along with Cu, Zn, Co, Ni, V metals from wall rocks of mica schist from the Dashiqiao and Gaixian Formations. Integrated mineral assemblage, sulfide texture, trace element and sulfur isotope signatures and geochronological constraints reveal the primary Paleoproterozoic SEDEX mineralization was intensively overprinted by later metamorphism and Mesozoic magmatic hydrothermal events for the Pb-Zn deposits in the Qingchengzi ore district.

* Corresponding authors.
E-mail addresses: winneduan@126.com (X. Duan), zengqingdong@mail.igcas.ac.cn (Q. Zeng).

https://doi.org/10.1016/j.oregeorev.2023.105829
Received 28 September 2023; Received in revised form 12 December 2023; Accepted 13 December 2023
Available online 19 December 2023

1. Introduction

Many sediment-hosted (SHMS), volcanic-hosted massive sulfides (VHMS) and other Pb-Zn deposits in orogenic belt are often reworked by later metamorphism and deformation. Examples include the Paleoproterozoic SEDEX Pb-Zn deposits in Australia (Bodon, 1998; Large et al., 2005; Gadd et al., 2016), and the deformed VHMS deposits such as Ashele Cu-Zn, Tiemurt Pb-Zn-Cu and Keketale Pb-Zn(-Ag) deposits in Chinese Altay (Zheng et al., 2016; Yu et al., 2020). Later metamorphism can induce recrystallization, annealing, brecciation or partial melting of sulfides, which leads to significant remobilization of metals (e.g., Ge, Ga, In, Cd, Cu) through intra-grain diffusion, mineral dissolution-precipitation, and transport of sulfide melt (Mishra and Bernhardt, 2009; Reiser et al., 2011; Lockington et al., 2014; Yu et al., 2020; Tiu et al., 2021). For example, Cugerone et al. (2021) suggested that dynamic recrystallization during metamorphism led to remobilization of Ga, Ge and Cu out from sphalerite crystal lattice, forming Ge minerals. Yu et al. (2020) reported mineral-scale element (Cu, Zn, Ag, Sb, Pb) remobilization, as well as variations of sulfur and lead isotopic compositions for sulfides hosted in the greenschist to lower amphibolite facies of the metamorphosed Keketale VHMS Pb-Zn(-Ag) deposit. In addition, late-stage magmatism can also cause significant modification of early Pb-Zn mineralization. Examples include the Hehuashan Pb-Zn deposit which composes a Triassic MVT mineralization overprinted by the Cretaceous magmatic-hydrothermal mineralization (Liu et al., 2021), the Laochang Pb-Zn-Ag deposit which reflects overprinting of the Carboniferous VHMS-type mineralization by the Eocene porphyry-skarn mineralization (Meng et al., 2018), and the Qingchengzi Pb-Zn deposits which document primary Paleoproterozoic SEDEX mineralization overprinted by later regional metamorphism and further modified by Mesozoic magmatic hydrothermal events (Duan et al., 2017; Zhou et al., 2020). In summary, multi-stage mineralization occurs in a significant part of mineral deposits, and in some cases, upgrades ore grade and reserves. However, discerning the individual stages of mineralization has been challenging because the overprint of late stage mineralization often obliterates early stage mineralization features, and induces reactivation-remobilization-deposition of metals which causes chemical heterogeneity of ore minerals.

Sulfide textural and chemical heterogeneity are common in those superimposed deposits (Cugerone et al., 2021), thus providing an option for distinguishing the individual stages of mineralization that form the multiple growth textures of sulfides. By using *in-situ* micro-scale analytical techniques, such as the EMPA and LA-ICP-MS element mapping, it is possible to constrain the compositional texture of sulfide minerals. For example, the LA-ICP-MS element mapping has been widely applied to reveal multigenerational growth history of minerals under the influence of later metamorphic events or hydrothermal activity and to understand the associated coupling relationship among elements (Large et al., 2009; Cook et al., 2009; Zhou et al., 2019; Thomas et al., 2011). Application of LA-ICP-MS element mapping of sulfides from reworked

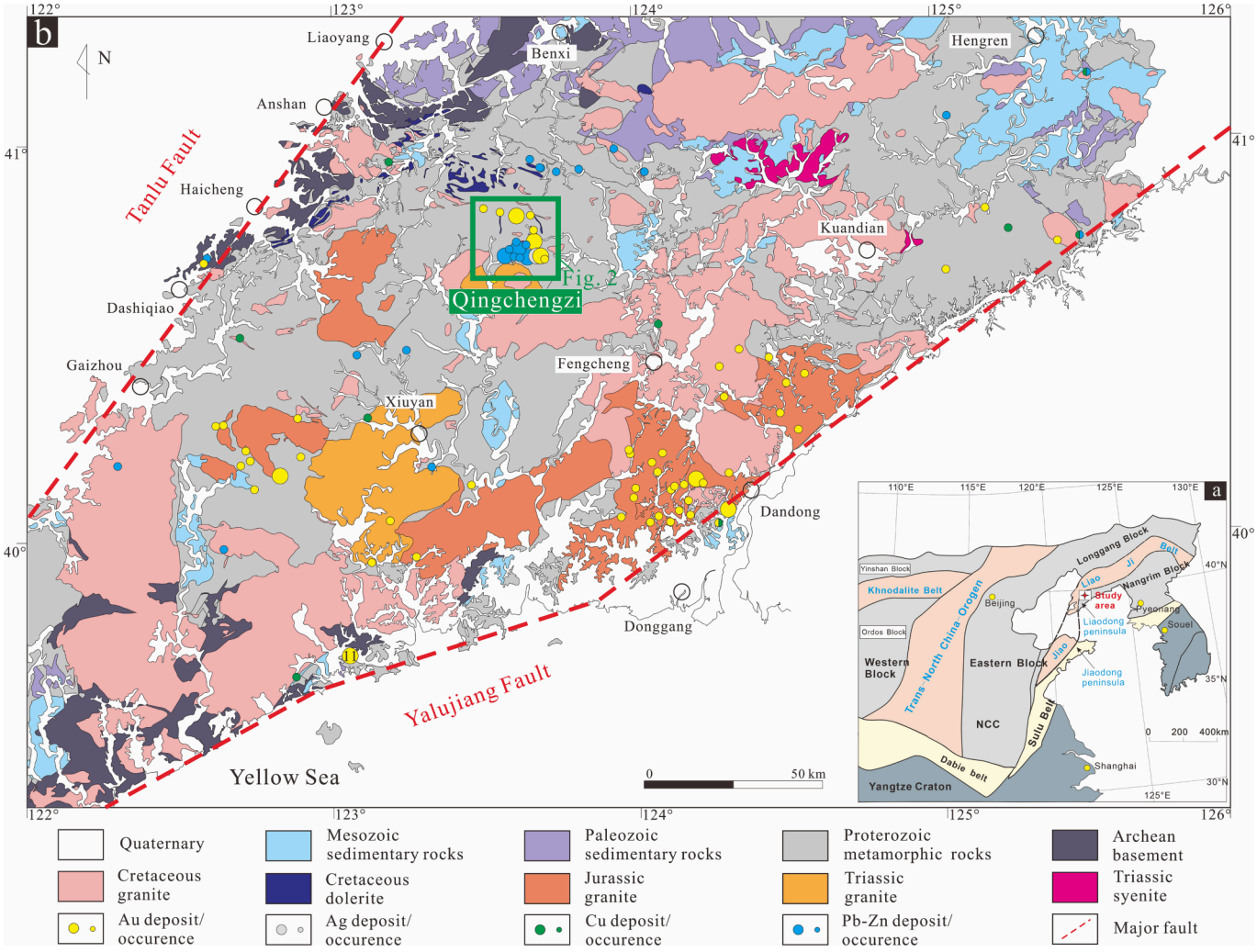

Fig 1. (a) Geological sketch map of the North China Craton (NCC), illustrating the tectonic location of the Jiao–Liao-Ji Belt; (b) Geological map of Liaodong region (after Zeng et al., 2019).

SEDEX and VHMS deposits include Gadd et al. (2016), in which element mapping revealed multigenerational growth of pyrite and distinguishes involvement of depositional, hydrothermal and metamorphic fluids. Thus, the textural and chemical composition of sulfide minerals revealed by *in-situ* analysis, together with well-defined paragenetic relationship and geochronology, have been shown to discern metamorphic and hydrothermal stages of mineralization that overprint early sedimentary mineralization (Marshall and Gilligan, 1993; Wagner et al., 2007; Cook et al., 2009; Gadd et al., 2016).

The Qingchengzi ore district in Liaodong Peninsula, northern China, hosts several reworked Pb-Zn deposits, which are characterized by superimposed multi-stage mineralization with different types of sulfides. The ore district contains 12 Pb-Zn deposits and several Au-Ag deposits (Fig. 1). The genesis of those Pb-Zn deposits is still controversial, with two prevailing models being proposed. The first model emphasizes sedimentary exhalative-(metamorphic) mineralization, which is related to the Paleoproterozoic rifting and the collisional orogenic event of the Jiao-Liao-Ji Belt (Zhang, 1984; Liu et al., 2007; Song, 2010). The second model argues that there are multiple mineralization events and the hydrothermal enrichment associated with the Mesozoic magmatic events plays a crucial role (Jiang and Wei, 1989; Duan et al., 2017; Zhou et al., 2020). Zhou et al. (2020) conducted sulfide trace element analysis of the stratiform ores from the Zhenzigou Pb-Zn deposit and concluded a multi-stage mineralization history for the Zhenzigou deposit. However, the work was based on a very limited number of samples, and a comprehensive study is required to obtain more representative results for the Qingchengzi ore district. Besides, several inconsistent ages were reported for the Pb-Zn mineralization, including a Paleoproterozoic age (1798 ± 8 Ma, Ma et al., 2016) and several Mesozoic ages varying from early Cretaceous, to late Jurassic and Late Triassic (Yu et al., 2009; Xu et al., 2020; Wang et al., 2020). How these ages correspond to the different stages of mineralization in the Qingchengzi ore field is still unclear. This study investigated the compositional texture of pyrite and sphalerite from the Zhenzigou, Diannan, Xiquegou and Erdao Pb-Zn deposits within the Qingchengzi ore district by *in-situ* trace element and sulfur isotopic analyses. Together with newly acquired geochronological constraints by U-Pb dating of apatite and zircon in the associated granite porphyry, we aim to establish a geochronology framework for the Pb-Zn mineralization in the Qingchengzi ore district, and within this frame further distinguish the superposed multiple mineralization events and determine the source of metals and sulfur. The impact of superposed mineralization on sulfide geochemistry is further discussed to understand micro-scale metal mobility during regional metamorphism and fluid-rock interactions.

2. Regional geology

The Qingchengzi polymetallic ore district is located in the Dandong city, Liaodong Peninsula in Northern China. The supracrustal rocks of Liaodong region mainly consist of Precambrian metamorphosed volcanic-sedimentary sequences and voluminous volcanic and magmatic intrusions. The Precambrian sequences include the Archean diorites, tonalities and granodiorites and the overlying Liaohe Group. The Liaohe Group is a suite of metamorphosed volcanic-sedimentary successions composed of a lower bimodal volcanic sequence, a middle carbonate sequence, and an upper pelite-rich sequence and is subdivided into Langzishan, Li'eryu, Gaojiayu, Dashiqiao and Gaixian Formation from bottom upwards. The Liaohe Group was deposited at 2.24–2.02 Ga and underwent greenschist- to lower amphibolite-facies metamorphism at 1.93–1.85 Ga (Wan et al., 2006; Luo et al., 2008). Magmatic activities in the region were mainly documented by Paleoproterozoic and Mesozoic magmatic rocks. The Paleoproterozoic granitoids comprise biotite monzogranitic gneiss, porphyritic monzogranite, granite, and alkaline syenite, as well as minor mafic intrusions composed of gabbro and dolerite (Li and Zhao, 2007; Tam et al., 2011). Mesozoic magmatic rocks can be divided into three stages: (1) the Late Triassic magmatic rocks (233–212 Ma), which are composed of alkaline intrusions and associated mafic rocks, as well as granites with enclaves, (2) the Jurassic magmatic rocks (180–156 Ma), including dominantly monzogranite and subdominant tonalite and diorite, all of which have experienced ductile deformation, and (3) the Early Cretaceous intrusions (131–117 Ma) which are the most widespread magmatic rocks and include undeformed to slightly deformed diorite, granodiorite, monzogranite and syenogranite (Wu et al., 2005).

Regionally the district has underwent multiple tectonic events, including the Paleoproterozoic collisional orogenic event forming the Jiao-Liao-Ji orogenic belt and subsequent Mesozoic tectonic events. The Jiao-Liao-Ji Belt, which lies at the eastern margin of North China Craton (NCC), is a Paleoproterozoic collisional orogenic belt between the Longgang Block and the Nangrim Block (Li and Zhao, 2007; Fig. 1a). Although the tectonic model (continental rifting vs. the arc-continent collision model) are still in debate, the region underwent collision at 1.9–1.85 Ga which induced metamorphism and deformation of the Liaohe Group and Paleoproterozoic granitoids. Three deformation events were recognized: the primary sedimentary layering (S_0) of the Liaohe Group was deformed to mesoscopic to small-scale cascading folds in D1 deformation. The D_2 deformation generated crenulation cleavages and vertical asymmetric folds. The D_3 deformation led to the formation of the vertical, open and superposition folds in the Dashiqiao Formation and regional NWW folds and a series of NWW thrust faults (Li et al., 2005; Tian et al., 2017). The studied region was reactivated during the Mesozoic and impacted by the subduction-collision event of the Yangtze Block and the NCC in the early Mesozoic, followed by the subduction of the Izanagi plate from the east in the Jurassic, and subsequently large-scale extension associated with the NCC thinning and destruction in the Cretaceous.

The prolonged tectonic evolution history has resulted in the Liaodong Peninsula being rich in diverse types of metallic resources including numerous Pb-Zn, Au-Ag, Fe and U deposits. The representative large deposits include the Qingchengzi Pb-Zn ore district, Baiyun and Wulong Au-Ag deposits, and the Liangshanguan uranium deposit (Song, 2010; Zeng et al., 2019). In addition, the region hosts abundant nonmetallic resources including abundant strata-bound graphite, magnesite, talc, and boron deposits, e.g., the Haicheng magnesite deposit, the Houxianyu and Wengquangou borate deposit (Dong et al., 2016, 2017). The uranium deposits and the B, Fe deposits are hosted in the Langzishan Formation and the Li'eryu Formation. The Pb-Zn and magnesite deposits are mainly hosted in the Dashiqiao Formation whereas the Au-Ag deposits are dominantly hosted in the Gaixian Formation regionally.

3. Deposit geology

The Qingchengzi ore district is a Pb-Zn-Au-Ag polymetallic ore district with more than 10 Pb-Zn deposits with total proven metal reserves of 150 Mt Pb + Zn(Fig. 2a). The representative deposits include the Zhenzigou, Diannan, Erdao Pb-Zn deposits and Xiquegou, Nanshan, Benshan Pb deposits. In addition, there are five Au-Ag deposits (i.e., the Xiaotongjiapuzi, Baiyun, Linjiasandaogou Au deposit and the Gaojiabaozi Ag-Au deposit) with a total 200 t Au and 2000 t Ag reserves. This study mainly focuses on the Pb-Zn deposits within the ore district.

The Paleoproterozoic *meta*-volcanic-sedimentary rocks of Liaohe Group is the most important ore-bearing rocks. The outcrops of Liaohe Group in the Qingchengzi ore district mainly include the Gaojiayu Formation, Dashiqiao Formation and Gaixian Formation from bottom upwards, and they are composed of interbedded marble and mica schist (Fig. 2b). The Pb-Zn orebodies are primarily hosted in marble of the Dashiqiao Formation, whereas the Ag-Au orebodies are mainly hosted in the Gaixian Formation (Fig. 2b). Four stages of magmatic events occurred in the district during the Paleoproterozoic, the Late Triassic and the Jurassic, and Early Cretaceous, respectively. The Dadingzi monzogranite intruded at Paleoproterozoic with a zircon U-Pb age of

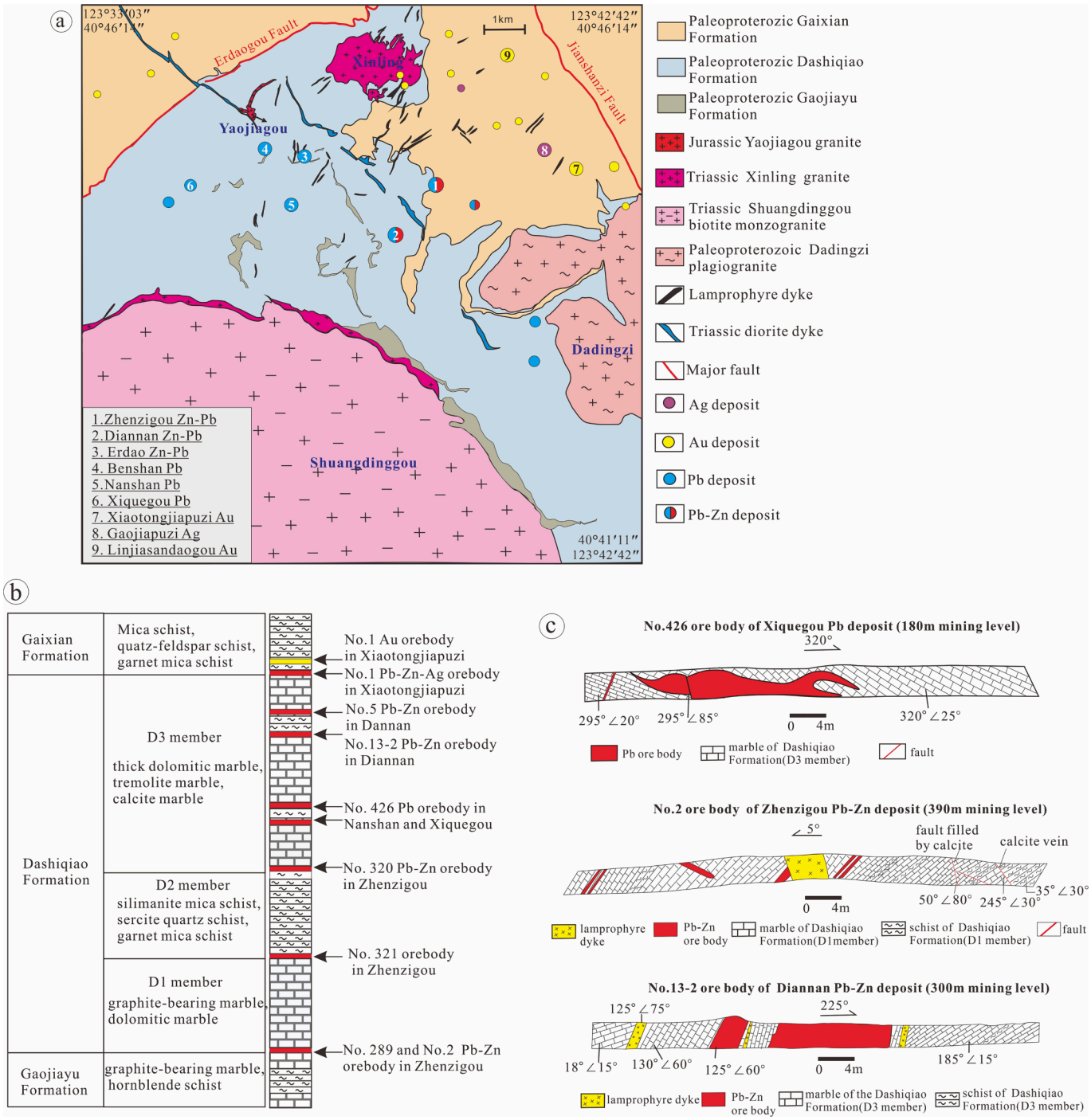

Fig. 2. (a)Geological map of the Qingchengzi ore district (after Duan et al., 2017); (b) Stratigraphic section of the Qingchengzi ore district and the distribution of orebodies; (c) Sketch of orebody occurrences at underground tunnel in the Zhenzigou Pb-Zn, Diannan Pb-Zn and Xiquegou Pb deposit.

~1869 Ma (Song et al., 2016). The Late Triassic magmatism was intensive, and formed intrusions including the Xinling granite porphyry (226 Ma, Duan et al., 2014), the Shuangdinggou biotite monzogranite (224 Ma, Duan et al., 2014), the Xiquegou granite porphyry dyke (216 Ma, Sun et al., 2020a) and the diorite (220–214 Ma, Wu et al., 2005) and lamprophyre dykes. The widespread lamprophyre dykes intruded into the Liaohe Group and the emplacement age was reported to be ca. 226 Ma (zircon U-Pb age, Sun et al., 2020a) and 193–136 Ma ($^{40}Ar/^{39}Ar$ age; Wang et al., 2020). Lamprophyre dykes often show close spatial relationship with orebodies demonstrated by some orebodies crosscutting lamprophyre dykes and vice versa. The Jurassic and Cretaceous intrusions are represented by the ca. 165 Ma Yaojiagou granite (Duan, 2015) and ca. 128 Ma quartz porphyry (Sun et al., 2020a), respectively.

3.1. Mineralization styles

The Pb-Zn deposits in the Qingchengzi ore district display various ore types and mineralization styles (Fig. 2c) which could be categorized into two types, i.e., “strata-bound” and “vein-type”. The strata-bound orebodies occur predominantly as stratiform, manto to semi-horizontal sheets and less commonly as lenticular, podiform, and nodular shapes (Fig. 3a, b). The representative orebodies include the No. 2, No. 320 and

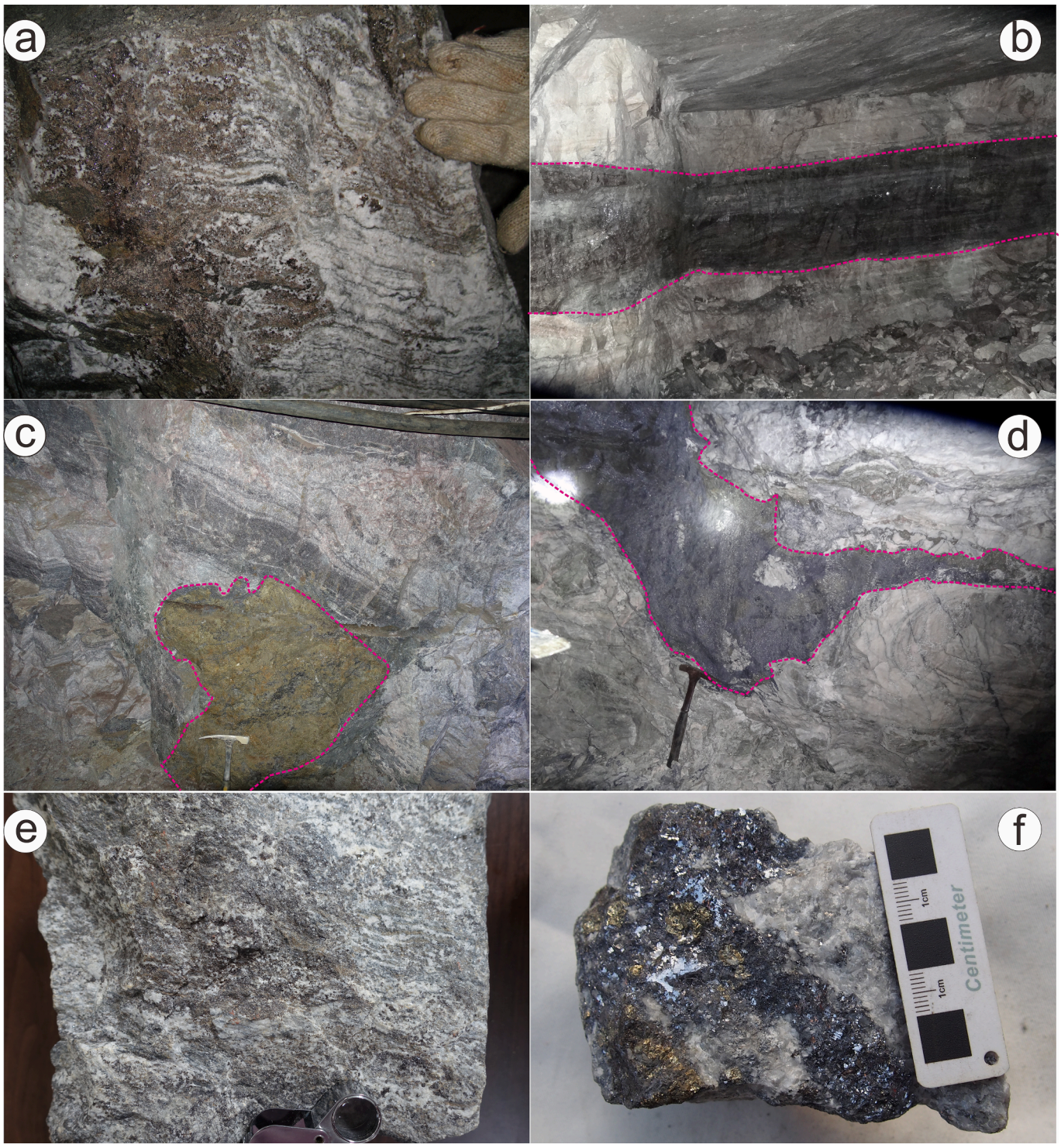

Fig 3. Photographs of different mineralization styles and ore types in the Qingchengzi ore field. (a) Lamellar orebody consisting of light brown fine-grained sphalerite from the Zhenzigou Pb-Zn deposit; (b) Extended tabular Pb–Zn orebody with width of 1–1.5 m and length of over 80 m, from the 270 m mining level of the Erdao Pb-Zn deposit; (c)Sacciform shaped orebody hosted in marble at the 300 m mining level of the Zhenzigou Pb-Zn deposit; (d) vein type orebodies hosted in marble at the 180 m mining level of the Xiquegou Pb deposit; (e)Stage-I stratiform ore sample comprised of laminated sphalerite and minor galena; (f)Stage-II massive ore sample comprised of galena, pyrite and minor dark brown sphalerite.

No. 321 orebodies in the Zhenzigou Pb-Zn deposit, which constitute a 2500 m-long and NW-trending ore belt striking NW 60°−70° and dipping to the NE with angles of 40°−70° (Duan et al., 2017). The vein-type generally refers to orebodies formed through open-space filling and occur in various shapes including steeply dipping veins, stock veinlets, and sacciform and breccia (Fig. 3c, d). In addition, in the Diannan Pb-Zn deposit, vein-type ores form massive sulfide pods and veinlets occur within or around a granite porphyry which was strongly altered with pervasive sericitization and silicification (Fig. 6a-c). Those orebodies often crosscut bedding and are structurally controlled by the NE-trending faults and occasionally occur at intersects of the main fault with favorable interlayer fractures. The major vein-type orebodies

include the No. 6404 and No. 426, which occur at the footwall of the No. 1 fault in the Xiquegou deposit. A series of vein-type orebodies collectively form en echelon arrays and constitute a 300-m-long, 300-m-deep and 50-m-wide ore belt that strikes NW and dipping to the NE with a pitch angle of 30°. Overall, the strata-bound orebodies contain higher Zn/Pb ratios than those of vein-type and the former is mainly hosted in marble at the lower sequence of the Dashiqiao Formation with minor occurrence in the Gaojiayu Formation whereas the latter is positioned at the upper sequence of the Dashiqiao Formation (Fig. 2b).

The primary metallic minerals of the Pb-Zn deposits include pyrite, sphalerite, galena, arsenopyrite, and chalcopyrite, as well as minor amounts of pyrrhotite, tetrahedrite, and argentite. The gangue minerals mainly consist of dolomite and subordinate calcite, quartz, sericite, chlorite, talc, graphite, serpentine and apatite. Two metallogenic stages are distinguished based on petrographic study, including the (1) stage-I sedimentary-metamorphic mineralization with mineral assemblages of light brown sphalerite, pyrite, chalcopyrite, galena, calcite, dolomite, graphite, serpentine, talc, apatite (Fig. 4a-d), and (2) stage-II magmatic-hydrothermal mineralization with mineral assemblages of dark brown sphalerite, pyrite, galena, arsenopyrite, chalcopyrite, dolomite, chlorite, sericite and quartz (Fig. 4e-h). There are slightly different mineral assemblages for Pb orebodies and Pb-Zn orebodies, the ore minerals of the former mainly include pyrite, galena, arsenopyrite and minor chalcopyrite (Fig. 4e), whereas the latter consists of sphalerite, pyrite, galena, and arsenopyrite (Fig. 4f). Stage-I mineralization is only partially retained and found in some part of strata-bound orebodies, in which only stratiform ores consisting of laminated light-brown fine grained sphalerite and disseminated pyrite recorded sedimentary mineralization (Fig. 3a,e). The metamorphic stage is recognized by the recrystallized sphalerite/pyrite associated with graphite and apatite in the manto or lenticular ores. Stage-II mineralization is prevailing over the ore district, forming dominantly vein-type ores and many of the strata-bound orebodies are modified products of former stage-I overprinted by stage-II mineralization. The sphalerite-galena-chalcopyrite ore veins in stage II cut through the graphite alignment and stage-I fine-grained sphalerite (Fig. 4g). These veins also crosscut the foliation of metamorphosed lithologies (Fig. 4h), indicating that vein-type mineralization occurred after the metamorphism.

3.2. Texture and paragenesis of pyrite and sphalerite

Pyrite is a common sulfide in the various ore types in Qingchengzi Pb-Zn deposits. In general, three types of pyrite are distinguished from the two stages of mineralization, namely the earliest sedimentary pyrite (Py0), pyrite developed in the sedimentary-metamorphic mineralization of stage-I (Py1), and pyrite developed in the magmatic-hydrothermal mineralization of stage-II (Py2). The Py0 is observed to occur in the barren marble and schist from the Gaixian and Dashiqiao Formation in absence of other sulfides (Fig. 4a). The medium-grained euhedral Py0 commonly shows a cubic shape and contains mineral inclusions of carbonate and other sulfides. Occasionally, the Py0 grains form aggregates parallel to the bedding of the host rock. The Py1 of stage-I mainly develops in stratiform ores and can be further divided into two sub-stages (Py1a and Py1b). The Py1a, which is only observed in limited lamellar ores, occurs as fine-grained pyrite grains disseminated in the marble and are mostly replaced by sphalerite (Fig. 4b). The Py1b is associated with fine-grained light brown sphalerite (Sp1) and graphite as well as apatite in the lamellar, manto, lenticular and stratiform orebodies. The Py1b is usually euhedral to subhedral (Fig. 4c) and also appears as elongated pyrite grains along the foliation of the mica schist (Fig. 4d). The stage-II pyrite (Py2) intergrows with coarse-grained brown sphalerite, galena, chalcopyrite and arsenopyrite and is widespread in veins, stock veinlets, sacciform, breccia and other vein-type orebodies in all the Pb-Zn deposits (Fig. 4e-h). The coarse-grained Py2 is usually subhedral-euhedral and commonly replaced by sphalerite and galena. LA-ICP-MS element mapping illustrates that it has multiple growth texture with compositionally distinct a core (Py2a) and a rim (Py2b).

Sphalerite can be divided into two types (Sp1 and Sp2) corresponding to the two mineralization stages. The Sp1 is mainly distributed in the lamellar and stratiform ores and can be subdivided into two subtypes (Sp1a and Sp1b). The Sp1a is fine grained, light brown in color, and disseminated in carbonates and only occurs in limited lamellar ores (Fig. 4b). The Sp1b is coarser grained compared to Sp1a and often is banded with graphite, or coexisting with apatite (Fig. 5a,b) in some of the strata-bound orebodies. The Sph2 is coarse-grained, subhedral to anhedral and coexists with Py2 and galena, arsenopyrite, chalcopyrite in the vein-type orebodies (Fig. 4f-h).

4. Sampling and analytical methods

The ore samples were collected to represent different mineralization styles (i.e., strata-bound and vein-type) from four Pb-Zn deposits, i.e., the Zhenzigou, Diannan, Erdao Pb-Zn deposits (Zn/Pb > 1) and Xiquegou Pb deposit (Zn/Pb < 1). Thin sections of the Pb-Zn ore samples were prepared for petrographic observation and subsequent *in-situ* geochemical and isotopic analyses. Pyrite and sphalerite from the different stages were analyzed by LA-ICP-MS and LA-MC-ICP-MS to obtain trace element compositions and S isotopes of the sulfide, respectively. Three stage-II pyrite grains were selected for trace element mapping. The microscopy scanning images of thin sections that display mineralogical characteristics of the measured samples are shown in supplementary Fig. S2–S6. Apatites coexisting with the stage-I sulfides (Fig. 5a, b) were selected for U-Pb dating and zircons from the granite porphyry that hosts Pb-Zn veins (Fig. 6a-c) were measured for U-Pb isotope dating by LA-ICP-MS. Besides, 24 samples of barren wall rocks including 9 marble and 15 mica schist from the Dashiqiao and Gaixian Formations were collected from underground tunnels distal from the Pb-Zn mineralization and were analyzed for their trace elements compositions by bulk ICP-MS solution analysis.

4.1. Apatite and zircon LA-ICP-MS U-Pb geochronology

The apatite U-Pb dating analyses were performed on an PlasmaQuant MS quadrupole ICP-MS from Analytik Jena with a 193 nm ArF excimer laser from New Wave Research at the Yanduzhongshi Geological Analysis Laboratories Ltd. Apatite standard MAD2 was used as the primary standard to calibrate the U-Pb geochronology of apatite. Apatite standard McClure Mountain and Kovdor were employed as secondary quality control standards. Instrument drift, mass bias and fractionation of the U-Pb ratio were corrected with a standard-sample bracketing method. The trace element U, Th and Pb concentrations of apatite were quantified using SRM610 as external standard and ^{44}Ca as the internal standard element assuming a stochiometric apatite composition. Each analysis on the apatite began with a 15-second blank gas measurement followed by a 40 s of analysis when the laser was switched on. The laser spot is 30 μm in diameter using a laser frequency at 7 Hz and a fluence of approximately 3.6 J/cm^2. The raw data was corrected offline employing ICPMSDataCal software (Liu et al., 2008) and ZSkits software. Common Pb was corrected using the ^{207}Pb-based correction method outlined in detail of Chew et al. (2014).

Zircon U-Pb dating analysis was conducted in the Institute of Geology and Geophysics, Chinese Academy of Sciences. An Agilent 7500a Quadrupole ICP-MS combined with Geolas Plus 193 nm laser ablation system was used for the U-Pb isotopic and elemental composition measurement. The laser diameter applied on samples was 40–60 μm and ablation time lasted for 80–120 s. The analysis used zircon 91,500 and GJ-1 as external standards for isotopic measurement. Whereas, for zircon trace element measurement, NIST610 was applied as the external standard and ^{29}Si as the internal standard. The ablation frequency applied was 8–10 Hz, with an energy density of 2.5 J/cm^2. A detailed description of the process can be found in Xie et al. (2008). The ^{207}Pb/^{206}Pb, ^{206}Pb/^{238}U, ^{207}Pb/^{235}U and ^{208}Pb/^{232}Th ratios were

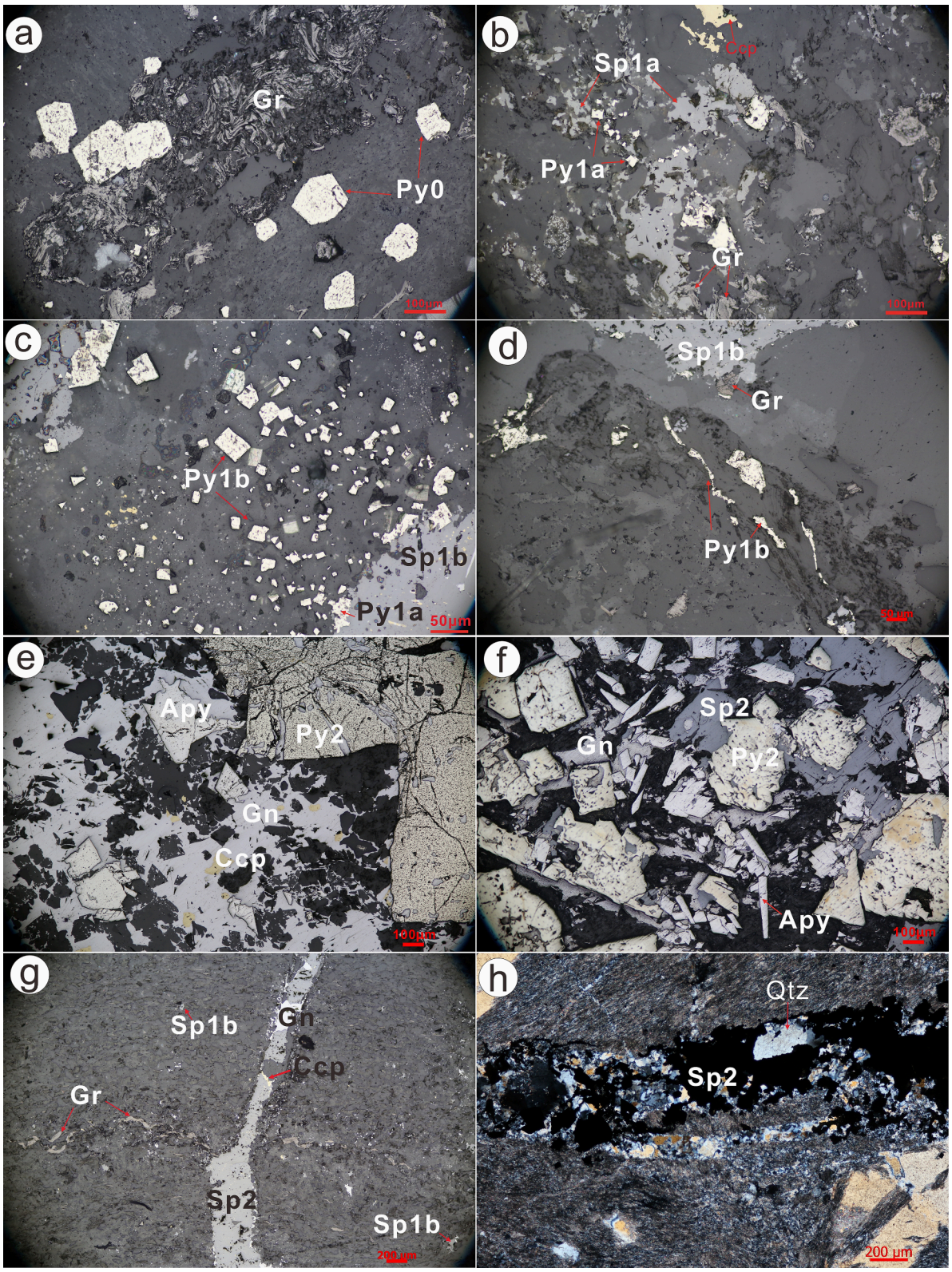

Fig. 4. Photomicrographs illustrating mineral paragenesis of two metallogenic stages of the Qingchengzi Pb-Zn deposits: (a) Sedimentary pyrite (Py0) grain in barren graphite-bearing marble of the Dashiqiao Formation; (b) The occurrences of the fine-grained sphalerite(Sp1a) and disseminated fine-grained pyrite; (c) Recrystallized euhedral pyrite grains (Py1b) in stratiform ores and anhedral Py1a which is replaced by Sp1b; (d) The elongated pyrite grains in stratiform ores; (e) anhedral arsenopyrite and chalcopyrite replaced by galena and (f) the euhedral prismatic arsenpopyrite crystals formed later than galena, pyrite and sphalerite; (g) Stage-II sphalerite (Sp2)-galena-chalcopyrite vein cuts through marble with linearly distributed graphite and fine-grained sphalerite(Sp1b); (h) Stage-II sphalerite (Sp2)-quartz vein cuts the foliation of the host schist; (h) Mineral assemblages of stage-II with coarse sphalerite, pyrite and arsenopyrite. Abbreviations: Sp: sphalerite, Py: pyrite, Gn: ganela, Gr: graphite, Apy: arsenopyrite; Qtz: quartz; Ccp: chalcopyrite.

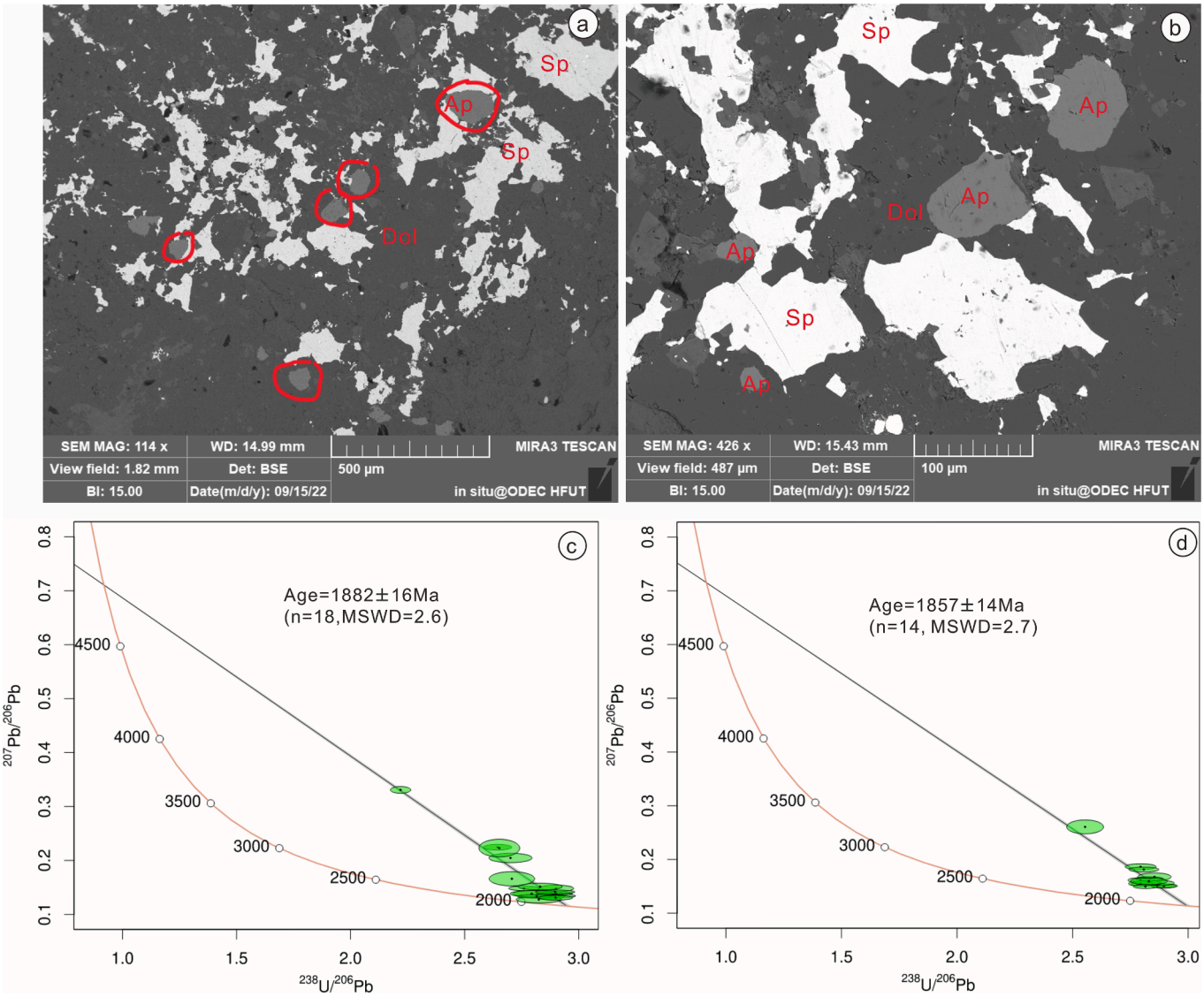

Fig. 5. (a-b)SEM images illustrating the apatite intergrowing with fine-grained stage-I sphalerite in stratiform Pb-Zn ores; (c-d) Tera-Wasserburg U-Pb concordia plots of apatite from two stratiform ore samples.

calculated and corrected by GLITTER, and lead corrections were applied when necessary by using the method proposed by Andersen (2002).

4.2. Sulfide LA-ICP-MS trace element analysis

Trace element abundance and distribution in the pyrite and sphalerite was determined by laser ablation (LA)-ICPMS at the Aarhus Geochemistry and Isotope Research platform (AGIR), Department of Geosciences, Aarhus University. For the pyrite spot analysis, an element list of ^{33}S, ^{34}S, ^{47}Ti, ^{55}Mn, ^{56}Fe, ^{57}Fe, ^{59}Co, ^{60}Ni, ^{63}Cu, ^{66}Zn, ^{71}Ga, ^{72}Ge, ^{75}As, ^{78}Se, ^{95}Mo, ^{107}Ag, ^{121}Sb, ^{125}Te, ^{197}Au, ^{208}Pb, ^{209}Bi was applied for the measurement. For the sphalerite spot analysis, ^{111}Cd and ^{115}In were added to the previous list used for pyrite measurement. For the elemental mapping, elements Co, Ni, Au, As, Cu, Zn, Ag, Sb, and Pb were analyzed to investigate their distribution patterns in the pyrite. The measurement was carried out using a 7900 Agilent quadrupole inductively coupled plasma mass spectrometer (ICPMS), coupled to a Resolution M155, 193 nm ArF Excimer laser from Resonetics. The sulfides were analyzed with a laser spot size of 12–60 μm. Sulfide standard MASS 1, basaltic glass BCR-2G and NIST 610 synthetic glass were applied as the reference materials. The raw data was processed in the Iolite 3.2 software (Paton et al., 2011).

4.3. Sulfide LA-MC-ICP-MS in-situ sulfur isotope analysis

In-situ sulfur isotopes of pyrite, arsenopyrite and sphalerite were measured on thin sections. The experiment was conducted in the Northwest University, China, using a Nu Plasma 1700 MC-ICP-MS, which is coupled with a RESOlution M−50 193 nm ArF excimer laser ablation system. A laser fluence of 3.6 J/cm^2, frequency of 3 Hz and laser spot size of 30 μm in diameter were applied during the measurement. The instrument drift and mass bias were corrected using a standard-sample bracketing approach with repeated measurements of standards before and after each sample. Time resolved analysis mode of data acquisition was used and each sample acquisition sequence comprised 30 s for background collection, 50 s for ablation signal collection, and 75 s for sample wash out. Py-4 ($\delta^{34}S_{V\text{-}CDT} = 1.7 \pm 0.3$ ‰) for pyrite and NBS123 ($\delta^{34}S_{V\text{-}CDT} = 17.8 \pm 0.2$ ‰) for sphalerite were used as external standards. In addition, the standards of Py-4, NBS123 and PTST-3 were inserted every 8 samples to monitor the accuracy of measurement. Detailed analytical procedures were described in Chen et al. (2017). The sulfur isotopic values $\delta^{34}S$ ($\delta^{34}S = [(^{34}S/^{32}S_{sample})/(^{34}S/^{32}S_{standard})\text{-}1]$

*1000) are reported relative to standard VCDT as $\delta^{34}S_{V\text{-}CDT}$ values.

4.4. Whole-rock trace element analysis

The bulk analyses of trace element composition of wall rocks were performed at the Laboratory of Beijing Research Institute of Uranium Geology, China. The whole-rock samples were crushed to less than 200 mesh. Approximately 50 mg of whole-rock powder was dissolved using HF-HNO_3 in screw-top Teflon beakers at 185 °C for two days, evaporated to dryness, redissolved in 7 M HNO_3, and re-evaporated to incipient dryness. Finally, the powder was dissolved in 2 % HNO_3 to get the analysis solution and the trace elements were measured with Finnigan Element II MC-ICPMS. USGS and Chinese National Rock Standards (BCR-2, GSR-1 and GSR-3) were used as reference material and the analytical precision was better than 10 %.

5. Results

5.1. Geochronological results

Apatite grains are commonly observed in the stratiform ores and are generally 30–100 μm in length and subhedral to euhedral in shape (Fig. 5). The apatites often either intergrow with or cuts through stage-I sulfides (Sp1 and Py1) which indicates their formation no earlier than stage-I mineralization. It is therefore possible to constrain a rough age of stage-I stratiform ores by age dating the apatite. The U-Pb isotopic compositions and age results of the analyzed apatite are presented in Supplementary Table 1 and illustrated in Fig. 5. The apatite grains from the stratiform ores successfully yield Tera-Wasserburg Concordia intercept ages (Fig. 5c, d). The 14 grains from sample ZZW-1 of the Zhenzigou Pb-Zn deposit yield a lower intercept age of 1857 ± 14 Ma (MSWD = 2.7), and the 18 apatite grains from sample 390–4 define a lower intercept age of 1882 ± 16 Ma (MSWD = 2.6). Those apatites are ubiquitous and occur as euhedral grains in the studied samples. The U-Pb ages are interpreted as the formation ages of apatite, and we estimate the stratiform mineralization in the Qingchengzi ore district to have formed in the Proterozoic.

In addition to the stratiform mineralization, massive sulfide pods and veinlets occur within or around a strongly altered granite porphyry in the Diannan Pb-Zn deposit (Fig. 6a-c), which implies that this type of mineralization happened later than the intrusion of granite porphyry. The zircons selected from the granite porphyry are columnar euhedral with length of 100–200 μm. The CL images of those zircons show regular oscillatory magmatic zoning, however, some zircons exhibits bright rims (Fig. 6d). The zircons contain 143–1094 ppm of U, 66–439 ppm of Th, and Th/U of 0.32–0.79. The high U and Th contents and Th/U(>0.4) ratios indicate a magmatic origin of the zircons (Hoskin and Schaltegger, 2003). The U-Pb data for the zircons from the granite porphyry are listed in Supplementary Table 2 and illustrated in Fig. 6d-f. In total, 20 points data were obtained for the sample and two sets of ages were determined. One group of zircons yield a Paleoproterozoic age at around 2290 Ma and most of those zircons have developed accretionary rims and some grains show enormously high contents of lead at the rims, which may reflect modification by later hydrothermal ore-forming fluids. The other group of zircons show a clustered coordinated young age with a $^{206}Pb/^{238}U$ weighted average age of 228.5 ± 5.8 Ma (n = 10, MSWD = 4.5) and no accretionary rims was observed. We conclude that the porphyry granite intruded at ~229 Ma, which confines the upper limit of the vein-type Pb-Zn mineralization in Qingchengzi. In combination with the apatite geochronology, at least two stages of Pb-Zn mineralization, namely the Paleoproterozoic and Mesozoic, are constrained.

5.2. Chemical composition of pyrite and sphalerite

The LA-ICP-MS trace element data of the pyrite and sphalerite are listed in Supplementary Table 3 and Table 4 respectively. The statistical ranges, averages and medians are illustrated in Fig. 7. The pyrite from the Qingchengzi ore district hosts variable amounts of As, Pb, Cu, Zn, Co, Ni, Ag, Sb and Au (Fig. 7a). Among those elements, arsenic is the most abundant trace element in most samples containing hundreds to 10^5 ppm. The subdominant elements are Cu, Zn, Co, Ni, Pb, Ag, Sb, which are in the range of tens to hundreds ppm. Gold and Bi are in the range of 10^{-3} to tens ppm.

The Py0 contains high contents of Co with IQR1-3 ranging between 1.07 and 240 ppm (interquartile range IQR1-3 describes the data ranges from 25th to 75th percentile and is used to report trace element concentrations hereafter in section 5.2) and Ni varying between 7.4 and 356 ppm, and low concentrations of Zn (0.93–2.55 ppm), As (31.94–468 ppm), Mn (0.18–2.96 ppm) and Au (0–0.19 ppm) compared to Py1a. In comparison, Py1a generally has high concentrations of Mn (3.76–24.3 ppm), Co (24.6–237 ppm), Ni (30.8–394 ppm), Zn (39.3–106 ppm) and As (1265–2908 ppm). The Py1b shows depletion in most trace elements such as Co (0.08–2.64 ppm), Ni (0.41–3.59 ppm), Au (0–0.29 ppm) and V (0.15–0.96 ppm) compared to Py1a. Stage-II pyrite (Py2) contains lower amounts of Co, Ni and Mn whereas it has higher concentrations of Au, As, Cu, Ag, and Sb compared to stage-I Py1 and Py0. Moreover, the core of stage-II pyrite (Py2a) contains higher contents of Cu (141–390 ppm), Zn (8.2–148 ppm) compared to the rim (Py2b), while the rim (Py2b) is relatively enriched in Au (0.97–5.49 ppm) and As (1442–8625 ppm).

The LA-ICP-MS results show the most abundant trace elements of sphalerite from the Qingchengzi ore district are Fe, Cd, Cu, Mn, and subordinately Ag, Pb, Sb, V, In, Ga (Fig. 7b). Stage-II sphalerite (Sp2) is enriched in most of the trace elements including Fe, Cd, Ag, In, Ga, Sb, and Pb compared to stage-I sphalerite. The Sp2 contains significantly higher Fe (43320–44900 ppm) and Cd (6568–11735 ppm) concentrations than those of Sp1 which has Fe contents of 14810–15260 ppm and Cd of 152–3715 ppm. The stage-I Sp1b displays lower concentrations of most elements including Cu, Cd, Ga, Sb compared to Sp1a. However, Sp1b shows much higher Mn (509–1896 ppm) compared to Sp1a which has Mn contents of 8.85–16.6 ppm.

5.3. Spatial distribution of trace elements in pyrite

LA-ICP-MS mapping of stage-II pyrite from the Diannan Pb-Zn and Zhenzigou Pb-Zn deposits shows a uniform distribution of Fe, S whereas the trace elements are unevenly distributed. Element distributions highlight four groups or element correlation clusters including Co vs. Ni, the Au vs. As, the Cu vs. Zn, and the Pb vs. Ag vs. Sb (Figs. 8, 9 and Supplementary Fig. S1).

The notable variations of Co, Ni, Au, As, Cu, and Zn reveal a clear core-rim texture for the vein-type pyrite. The core is irregular and enclosed by a pyrite overgrowth, forming a euhedral pyrite. The core shows a significant enrichment of Cu and Zn and a depletion of Co, Ni, Au and As, while the rim is strongly enriched in Au and As and weakly enriched in Co and Ni. Although Co and Ni display comparable distribution patterns with Au, As in Fig. 8, the variations of Co and Ni do not necessarily follow those of Au and As in either Fig. 9 or Fig. S1. For example, the Co and Ni is enriched as a thin layer at the outer edge of the Py2 grain, whereas Au and As enrichment display a much larger domain of the pyrite grain from the Diannan and Zhenzigou deposit (Fig. 9; Fig. S1). The distribution of Ag, Pb and Sb is different from those of Cu and Zn and the distribution pattern of those elements is not consistent among the different pyrite grains. They can be enriched either within the intra-grain fractures (Fig. 8) or concentrated in the inner core of pyrite which seemingly represents galena micro-inclusions (Fig. 9).

In addition, some pyrite grains record more complicated multigenerational growth texture, for example, pyrite from the Diannan Pb-Zn deposit reveals a inner core, which is depleted in Cu and enriched in V, likely represents the relicts of stage-I pyrite Py1b, however, this relict is not always preserved (Fig. 9).

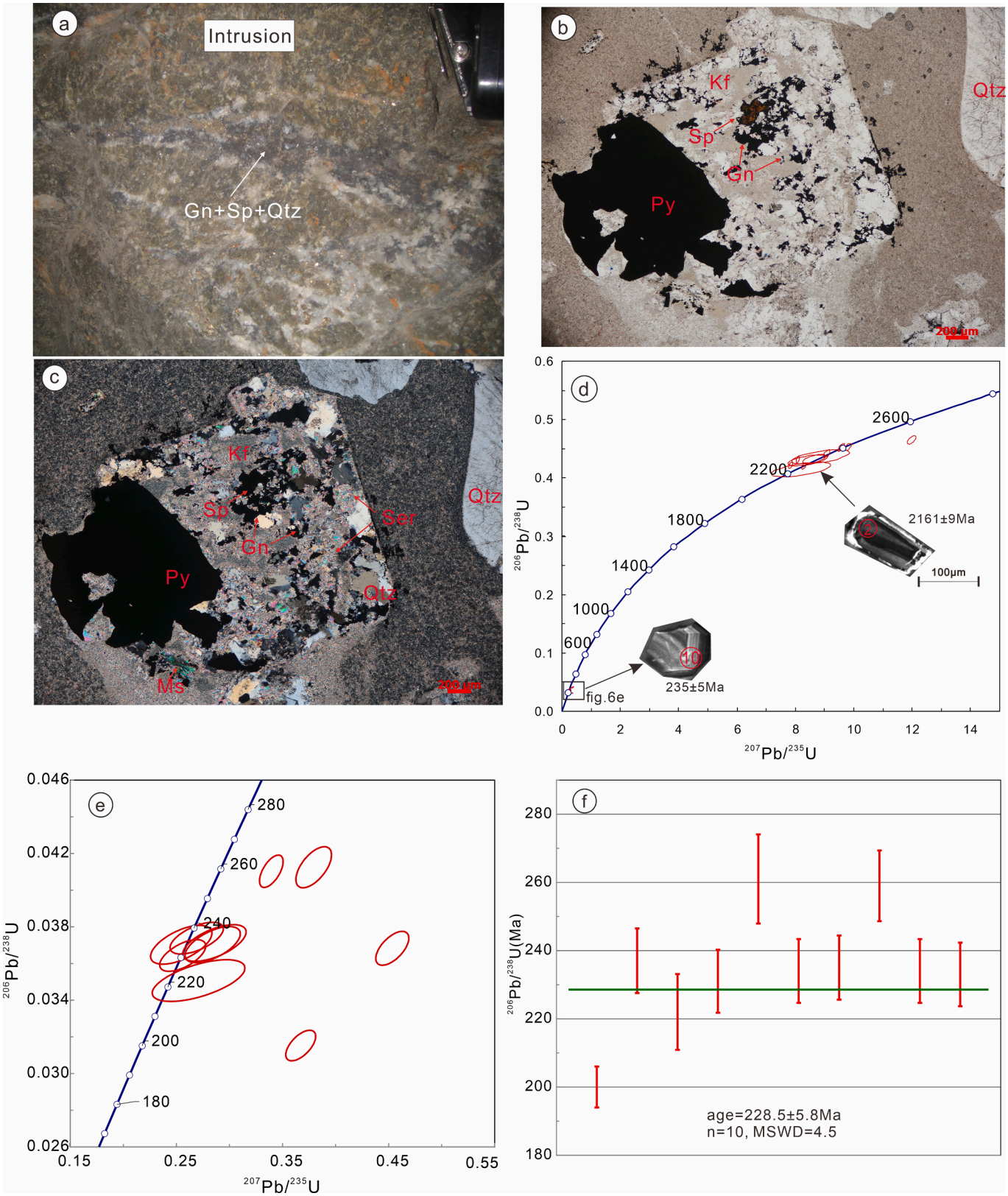

Fig 6. (a) Ore veins (galena + quartz) developed in sericitized granite porphyry, from the 360 m mining level of the Diannan Pb-Zn deposit; (b) Microphotograph of pyrite, sphalerite and galena distributed around the plagioclase phenocryst of the granite porphyry in Diannan Pb-Zn deposit, transmitted light (plane polarized); (c) cross polarized image of (b) showing strong alteration of plagiocalse with silicification and sericitization; (d) U-Pb concordia plot as well as CL images of two types of zircons from the granite porphyry in Diannan Pb-Zn deposit; (e) Enlarged view of U-Pb concordia plot of young zircons from the granite porphyry;(f) $^{206}Pb/^{238}U$ weight average age diagram of young zircons from the granite porphyry. Abbreviations: Sp: sphalerite, Py: pyrite, Gn: ganela, Ser: sericite; Ms: muscovite; Kf: k-feldspar; Qtz: quartz.

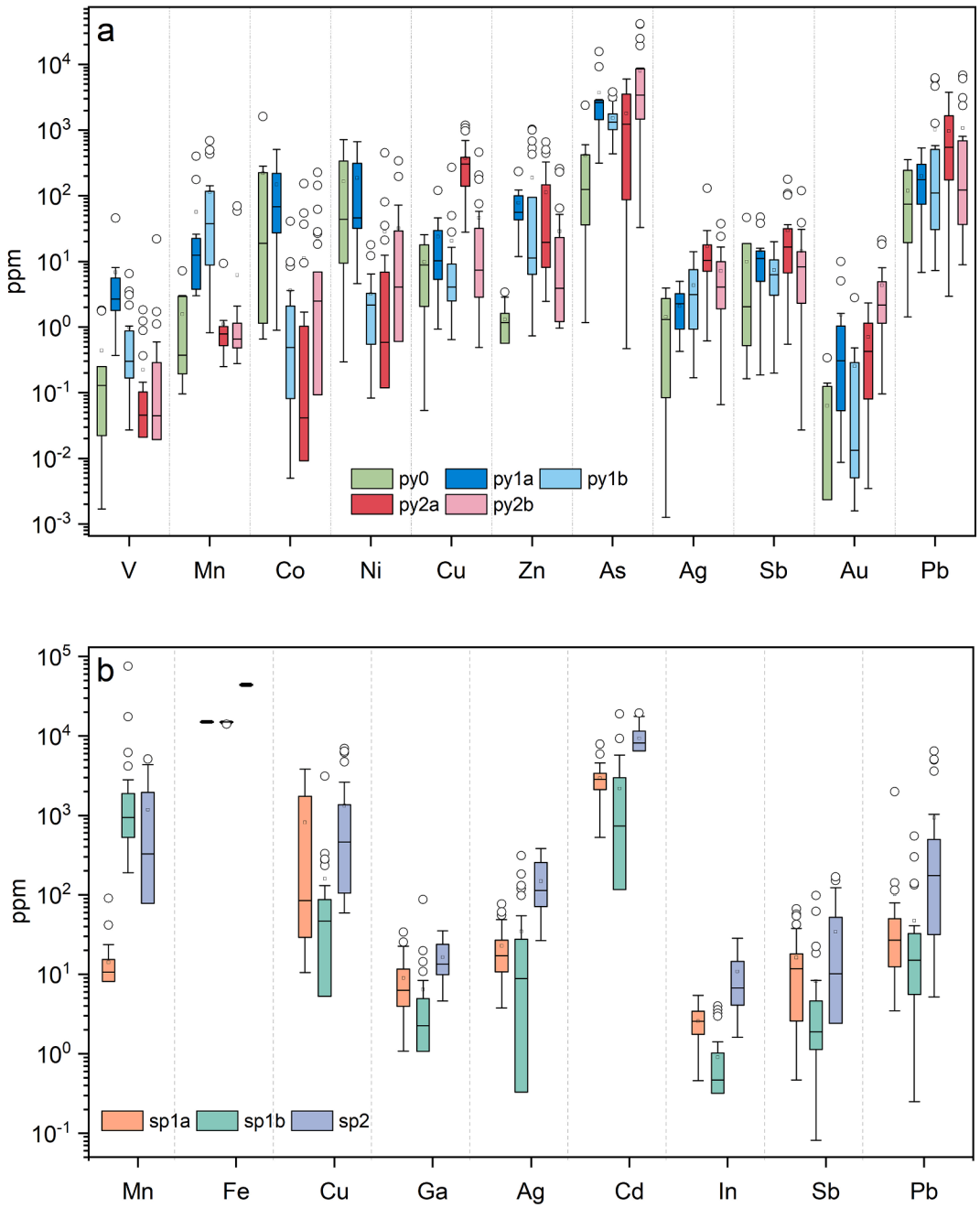

Fig. 7. Tukey box plot diagrams illustrating trace element compositions of pyrite (a) and sphalerite (b) in the Qingchengzi ore district. The lower whisker represents the interquartile range (IQR: box length) divided by 1.5, the lower part of the box the 25th percentile(IQR1), the upper part of the box the 75th percentile(IQR3), and the upper whisker represents IQR × 1.5. The square represents the mean, and the horizontal line represents the median and the open circles represent outliers (beyond 1.5IQR).

5.4. Sulfur isotopes of pyrite and sphalerite

In-situ sulfur isotope compositions of 12 arsenopyrite, 36 pyrite and 22 sphalerite from the ore samples and 6 sedimentary pyrite from Dashiqiao and Gaixian Formations are listed in Supplementary Table 5 and illustrated in Fig. 10. The $\delta^{34}S$ values of sedimentary pyrite from the Gaixian Formation (10.40–17.04 ‰) is higher than those of pyrite from the ore samples (4.10–9.37 ‰). More specifically, the stage-I pyrite Py1a shows $\delta^{34}S$ values of 7.70–9.37 ‰, which is higher than those of Py1b (4.10–6.56 ‰). Stage-II pyrite Py2a and Py2b, which is represented by the pyrite core and rim respectively, are similar in $\delta^{34}S$ values of 5.05–8.36 ‰. Sphalerite formed at the different mineralization stages has relatively concentrated $\delta^{34}S$ values, which is confined in the ranges of 7.80–9.07 ‰ for Sp1a, 5.40–7.08 ‰ for Sp1b and 5.22–8.15 ‰ for Sp2. Only arsenopyrite from the stage-II vein-type mineralization was analyzed for sulfur isotope composition, and the $\delta^{34}S$ values vary from 4.10 ‰ to 9.02 ‰, which are comparable to those for pyrite (Py2) and sphalerite (Sp2) formed in stage II.

5.5. Trace element compositions of host rocks

The schist from the Dashiqiao and Gaixian Formations are both elevated in Cu (5.43–252 ppm), Zn (34.2–213 ppm), Co(12.3–57.1 ppm), Ni(11–145 ppm) and V (56–330 ppm). The marble contains 0.9–14.1 ppm Cu, 7.6–29 ppm Zn, 0.8–4.5 ppm Co, 5.6–14.3 ppm Ni, and 5.9–21 ppm V. The hornblende schist from the bottom of the

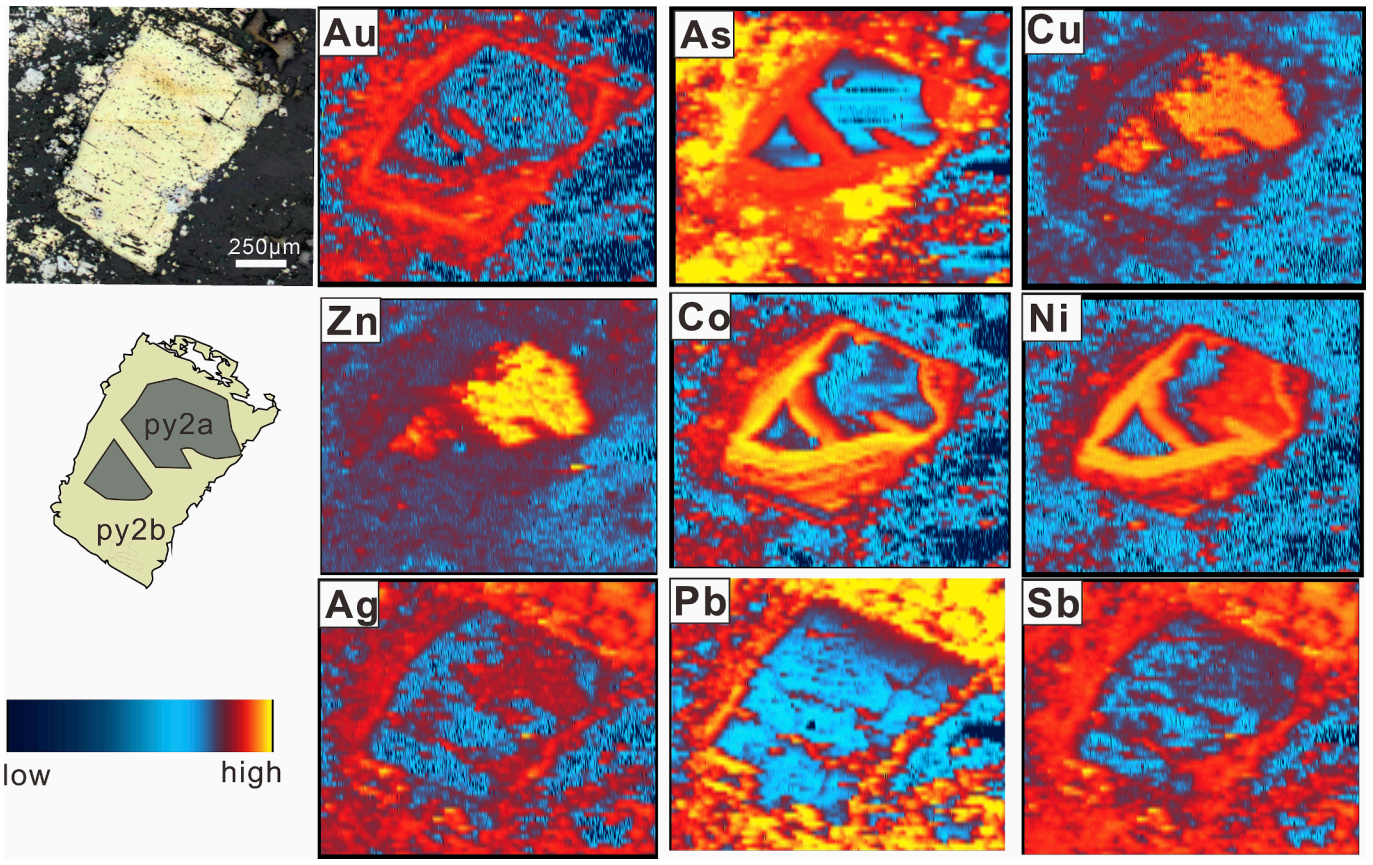

Fig. 8. LA-ICP-MS trace element mapping of one pyrite grain (Py2) from the Diannan Pb-Zn deposit, Qingchengzi ore district.

Dashiqiao Formation has higher V contents (59.1–330 ppm) than those of mica schist from the Dashiqiao and Gaixian Formations (56–153 ppm of V) whereas the mica schist from the Gaixian Formation contains the highest Co, Ni contents with 14.2–43.8 ppm and 11.7–138 ppm respectively(Supplementary Table 6).

6. Discussion

6.1. Multiple stages of mineralization

Previous studies in the field and petrographic observations and sulfide geochemistry all lead to the conclusion that the Qingchengzi Pb-Zn deposits are formed from multiple stages of mineralization (Jiang and Wei, 1989; Ma et al., 2013; Duan et al., 2017; Zhou et al., 2020). The new geochronology data we acquired from this study also suggest at least two stages of mineralization. The first stage is represented by the U-Pb age of apatite that coexists and crosscuts Sp1 and Py1 in stage-I, which is in the range of 1882–1857 Ma (Fig. 5). This suggests that the formation of stage-I sphalerite and pyrite was no later than 1.85 Ga, corresponding to the 1.93–1.85 Ga regional metamorphism pervading in the Liaodong region (Wan et al., 2006; Luo et al., 2008). The Paleoproterozoic mineralization is roughly consistent with an Rb-Sr isochron age of sphalerite at 1798 ± 8 Ma reported for the Zhenzigou Zn-Pb deposit (Ma et al., 2016). Petrographic evidence supporting a Paleoproterozoic mineralization includes the close intergrow and crosscutting relationship between the Sp1b/Py1b and coarse-grained graphite (Fig. 4b,g). Regionally, the Liaohe Group hosts a significant amount of graphite deposits which are considered to be formed through prograde metamorphism during the Proterozoic collisional orogeny (Zhu et al., 2021). In summary, the combined apatite geochronology and petrographic evidence constrains a stage of Paleoproterozoic Pb-Zn mineralization before or contemporary with the regional metamorphism during 1.93–1.85 Ga.

In addition to the Paleoproterozoic mineralization, a stage of Mesozoic mineralization is identified by the zircon U-Pb dating of the granite porphyry which hosts Pb-Zn veins. The zircons yielded a U-Pb age of 228.5 ± 5.8 Ma (Fig. 6), which indicates there is a stage of Pb-Zn mineralization later than 229 Ma. This stage of Pb-Zn mineralization can be related to the abundant existing geochronological data which suggest a Mesozoic Pb-Zn mineralization for the Qingchengzi area. The reported ages include 225–221 Ma confined by sphalerite Rb-Sr dating (Yu et al., 2009), 159–143 Ma determined by pyrite Rb-Sr dating (Xu et al., 2020), and $^{40}Ar/^{39}Ar$ dating of sphalerite and lamprophyre dykes (Wang et al., 2020) which reported three groups of ages (i.e., Late Triassic 224–193 Ma, late Jurassic 167–152 Ma, and early Cretaceous 138–134 Ma). The distinct groups of ages might suggest the Mesozoic mineralization further involves sub-stages of hydrothermal events in the Qingchengzi ore district.

This study has further distinguished different types of pyrite and sphalerite showing distinct composition, texture and mineral assemblages in Qingchengzi, which reflects the multi-stage mineralization. The Sph1 is lighter in color and contains lower Fe, Mn and In contents than the Sp2, which may be owing to a lower formation temperature. Both Mn and V tend to be concentrated in pyrite at low temperature (Maslennikov et al., 2009) and the decrease of Mn and V from Py1 to Py2 possibly suggests an increase in temperature of the ore-forming fluids. The increase of ore-forming temperature from stage I to stage II precludes an explanation of gradual cooling of a common fluid for the formation of sulfides in Qingchengzi, but rather indicates the involvement of two different fluids for the two stages of sulfide formation.

6.2. Implications from pyrite and sphalerite trace elements

The trace elements of Py1a from the Qingchengzi ore district show

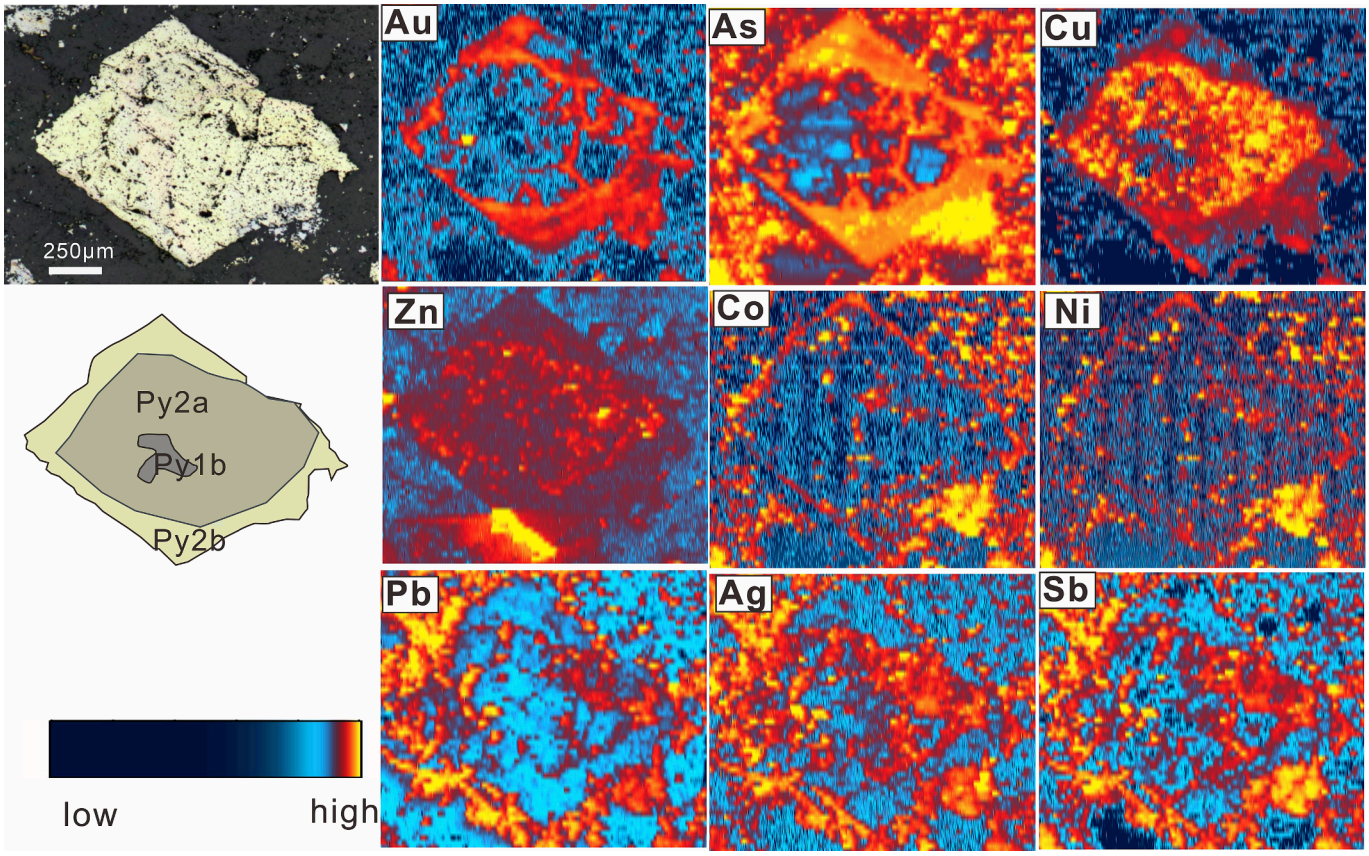

Fig. 9. LA-ICP-MS trace element mapping of one pyrite grain (Py2) from the Diannan Pb-Zn deposit, Qingchengzi ore district.

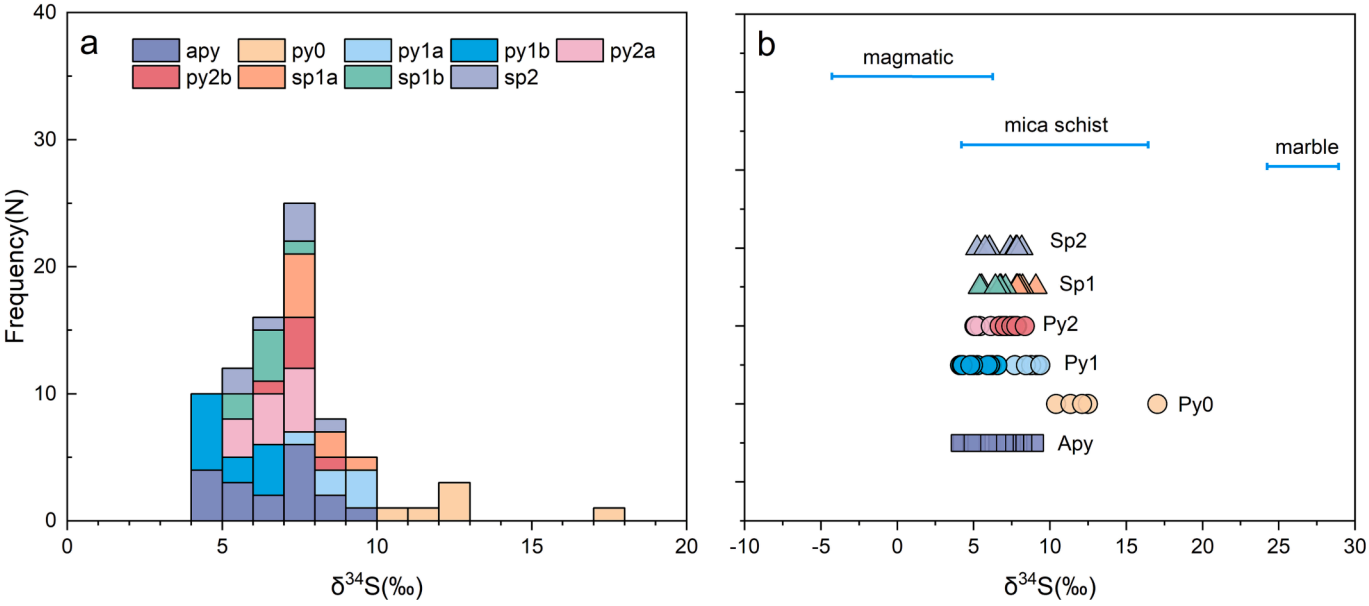

Fig. 10. (a)The histogram of sulfur isotope composition of sulfides from Pb-Zn deposits, Qingchengzi ore district; (b) $\delta^{34}S$ value ranges of different stages of sulfide in comparison with magmatic sulfur (Hoefs, 2009) and *meta*-volcanic-sedimentary rocks of the Dashiqiao and Gaixian Formations (Liu et al., 2022).

enriched Co, Ni, Mn, and V values, which is similar to those of the sedimentary Py0 but the former is more enriched in Zn. In general, pyrite from SEDEX Pb-Zn deposits and sedimentary pyrite share similar compositions for most trace elements, which is characterized by high concentrations of trace elements including Co, Ni, Cu and Zn (Gregory et al., 2019). This suggests that the Py1a and Sp1a are of SEDEX origin. The high Mn and V contents of Py1a may reflect a formation condition of low temperature with a sedimentary origin (e.g., Gadd et al., 2016). The high concentrations of Mn, Co and Ni of Py1a suggest that it was deposited in a relatively reducing environment, corresponding to sub-seafloor carbonate replacement. The incorporation of Mn into pyrite is redox dependent and an euxinic environment favors sequestering Mn by

pyrite (Huerta-Diaz and Morse, 1992). The notable higher Mn concentration of early pyrite suggests reducing conditions of its formation. The enrichment of Co and Ni in Py1a can be caused by two mechanisms. Firstly, in reducing environment, As(-I) tends to replace S(-II) which favors the substitution of ions with radii and charges similar to those of Fe(II), e.g., Co^{2+}, Ni^{2+}, Cu^{2+} and Zn^{2+} (Deditius et al., 2008). The second is that Co, Ni, and other bivalent transition metals are readily adsorbed onto organic matters which is broken down and released into pore water during sulfate reduction or late diagenesis (Berner et al., 2012).

The euhedral cubic grains and elongated grains along the foliation of the mica schist of Py1b suggest recrystallization and deformation (Fig. 4c, d), which is indicative of metamorphism under upper amphibolite facies (Tiu et al., 2021). Py1b is depleted in most of the trace elements compared to Py1a and is featured by lower Co, Ni, Cu, V, As, and Au contents but shows comparable high contents of Mn and Zn. It has been proposed that metamorphism can result in the loss of some trace elements, which are forced out of the pyrite crystal lattice at metamorphic grades higher than mid-greenschist facies (Large et al., 2009; Thomas et al., 2011; Gregory et al., 2019). The Sp1b coexisting with Py1b in the Zn-rich laminated ores is depleted in almost all the trace elements (e.g., Cu, Cd, In, Ag, Sb) but enriched in Mn compared to Sp1a. The depletion of most trace elements in Sp1b can be explained by recrystallization accompanied with elemental remobilization, a process which is facilitated by deformation and metamorphic fluids and leads to elemental remobilization from sphalerite crystal lattice into accessory minerals (e.g., Harlov et al., 2016; Yu et al., 2020; Cugerone et al., 2021). The enrichment of Mn in Sp1b is likely due to an increase in temperature and decrease in sulfur fugacity of the ore-forming fluids (Lusk et al., 1993; Keith et al., 2014). Furthermore, recrystallization of sphalerite could enhance the incorporation of Mn into sphalerite (Ramdohr, 1969; Lockington et al., 2014). The recrystallization process, which is associated with the dissolution of carbonate wall rocks during metamorphism has likely resulted in the higher Mn content in Sp1b (Tiu et al., 2021). In conclusion, the depletion of Co, Ni, Cu, V, Au, Cd and In of Py1b and Sp1b reflects recrystallization of sulfide induced by the 1.93–1.85 Ga metamorphism in the Qingchengzi ore district.

The stage-II sulfides (Py2 and Sp2) are more enriched in metals compared to stage-I sulfides, as illustrated by higher Cu, Ag, Au, As, Sb, Pb of Py2 than those of Py1 and more abundant in Cu, Ga, In, Sb, Pb, Ag in Sp2 than in Sp1 (Fig. 7). The distinct chemistry of stage-II sulfides implies they were precipitated from different fluids, and are associated with the Mesozoic magmatic-hydrothermal processes in the Qingchengzi ore district. Py2 grains from the different deposits of the Qingchengzi ore district display a common growth texture featuring an irregular core of enriched Cu and Zn with an overgrowth rim of enriched Au, As, Co, and Ni. The contrasting composition of core and rim indicates they are formed from two individual hydrothermal events. Considering the geochronological constraints, the Cu and Zn enriched core is most likely formed by the Triassic magmatic derived fluids whereas the rim is associated with the Jurassic or Early Cretaceous magmatic-hydrothermal fluids. The Jurassic and Early Cretaceous magmatic fluids are reported to be fertile in Au and As, and are responsible for forming the Linjiasandaogou Au deposit, Baiyun Au deposit and Xiaotongjiapuzi Au deposits within the Qingchengzi ore district (Sun et al., 2020b, 2022, 2023). Therefore, it's assumed that Au and As enrichment in the rim of Py2 are attributed by magmatic-hydrothermal influx.

6.3. Possible source of sulfur and metals

The $\delta^{34}S$ values of sulfide minerals can represent the total sulfur in the hydrothermal fluids in systems with medium–low temperature, low fO_2, and simple mineral associations (Ohmoto, 1972; Hoefs, 2009). The sulfide minerals in Qingchengzi are relatively simple, mainly including sphalerite, galena, pyrite, arsenopyrite, and chalcopyrite. Sulfate minerals or hematite occur rarely. This suggests that the measured $\delta^{34}S$ values of the sulfides minerals are approximately equal to or slightly higher than the bulk sulfur isotope compositions of related fluids.

The Py0 in the barren mica schist, which represents *syn*-sedimentary deposition, shows heavier $\delta^{34}S$ values (10.4–17.04 ‰) compared to sulfides in ores (4.10–9.37 ‰). Contemporary $\delta^{34}S$ values of seawater sulfate are 14–21 ‰ in the Proterozoic (Canfield and Raiswell, 1999). The positive $\delta^{34}S$ values of Py0 and the narrow difference between Py0 and seawater sulfate strongly support that the sulfur was sourced from reduction of seawater sulfate through thermochemical reduction (TSR), which generally result in fractionation by −10 to 0 ‰ (Orr, 1974). Bacterial sulfate reduction (BSR), which can produce fractionation by −60 to −15 ‰ (Goldhaber and Kaplan, 1975), may have played a limited role in producing the reduced sulfur in the Qingchengzi ore district. It should be noted that reported $\delta^{34}S$ values of pyrites in marble and mica schist of the Dashiqiao and Gaixian Formation span from 22.9 ‰ to 26.9 ‰ and from 3.3 ‰ to 16.1 ‰ respectively (Liu et al., 2022). This implies heterogeneity of sulfur isotopes within the sedimentary sequences of the Liaohe Group, thus, although Py1(Sp1) shows different $\delta^{34}S$ values compared to Py0, it is suggested that sulfur of stage-I sulfides probably are derived from sulfate reduction. The mica schist is enriched in metals such as Co, Ni, Cr, V and Cu and Zn (Supplementary Table 6) and the metals of stage-I sulfides are possibly leached from the rocks of the Liaohe Group.

The $\delta^{34}S$ values of sulfides (Py2, Sp2 and arsenopyrite) in the magmatic-hydrothermal stage-II range between 4.10–9.02 ‰, which is slightly higher than that of magmatic sulfur (−5–+5‰, average 0 ‰, Hoefs, 2009). Thus, magmatic sulfur is unlikely to be the only sulfur reservoir. We suggest that there is mixing of magmatic sulfur and sulfur leached from *meta*-volcanic-sedimentary rocks in the Liaohe Group which has a wide range of $\delta^{34}S$ values of 0.9–20.3 ‰ (Fig. 10). Besides, the Cu, Zn contents increase but Co, Ni contents decrease linearly along with decreasing $\delta^{34}S$ values for pyrites from sedimentary origin to lamellar ores, and to vein-type ores (Fig. 11). This correlation is best explained by two-end-member mixing with the magmatic fluids of isotopically lighter $\delta^{34}S$ values and enriched Cu, Zn as one end-member and *meta*-volcanic-sedimentary rocks of heavier $\delta^{34}S$ values and enriched Co, Ni as the other end-member. When fluid-rock interaction proceeded with the migration of magmatic fluids, the hydrothermal fluids leached heavy sulfur along with Cu, Zn, Co, Ni, V metals from wall rocks of mica schist from the Dashiqiao and Gaixian Formations. Although Cu and Zn may have been partly leached from *meta*-sedimentary rock, the metals of Cu and Zn of stage-II were predominantly sourced from magmatic fluids as inferred from Fig. 11a,b. However, it is assumed that Co, Ni were largely contributed by *meta*-volcanic-sedimentary rocks (Fig. 11c, d). On the other hand, the Liaohe Group was reported to contain very low concentrations of gold (1.2–3.9 ppb by Yang et al., 2015 and average of 0.19 ppb Au by Wei et al., 2021) and could not serve as the important source for Au. The gold was probably mainly from magmatic fluids as suggested by Sun et al. (2022,2023).

6.4. Mineralization processes of Qingchengzi Pb-Zn deposits

The paragenetic sequences of sulfides combined with geochronological constrains, and sulfide trace element composition and distribution, consistently suggest a multi-stage mineralization process for the Pb-Zn deposits in the Qingchengzi area (Fig. 12). In the Paleoproterozoic, the Qingchengzi area was in a rifting environment, where a sequence of volcanic-carbonate-pelite-rich sedimentary sequence as Liaohe Group at 2.2–2.0 Ga was deposited. Early diagenetic pyrite (Py0) was formed in reducing pore water with enriched Co and Ni contents. Zinc-Pb mineralization was mostly initiated in the first stage, when fine-grained sulfides were formed. The fine-grained nature of stage-I sulfides suggest rapid precipitation due to the mixing of seawater with metalliferous fluids. The pyrite (Py1a) and sphalerite (Sp1a) were formed through sub-seafloor replacement with ore metals (Zn, Cu) replacing the

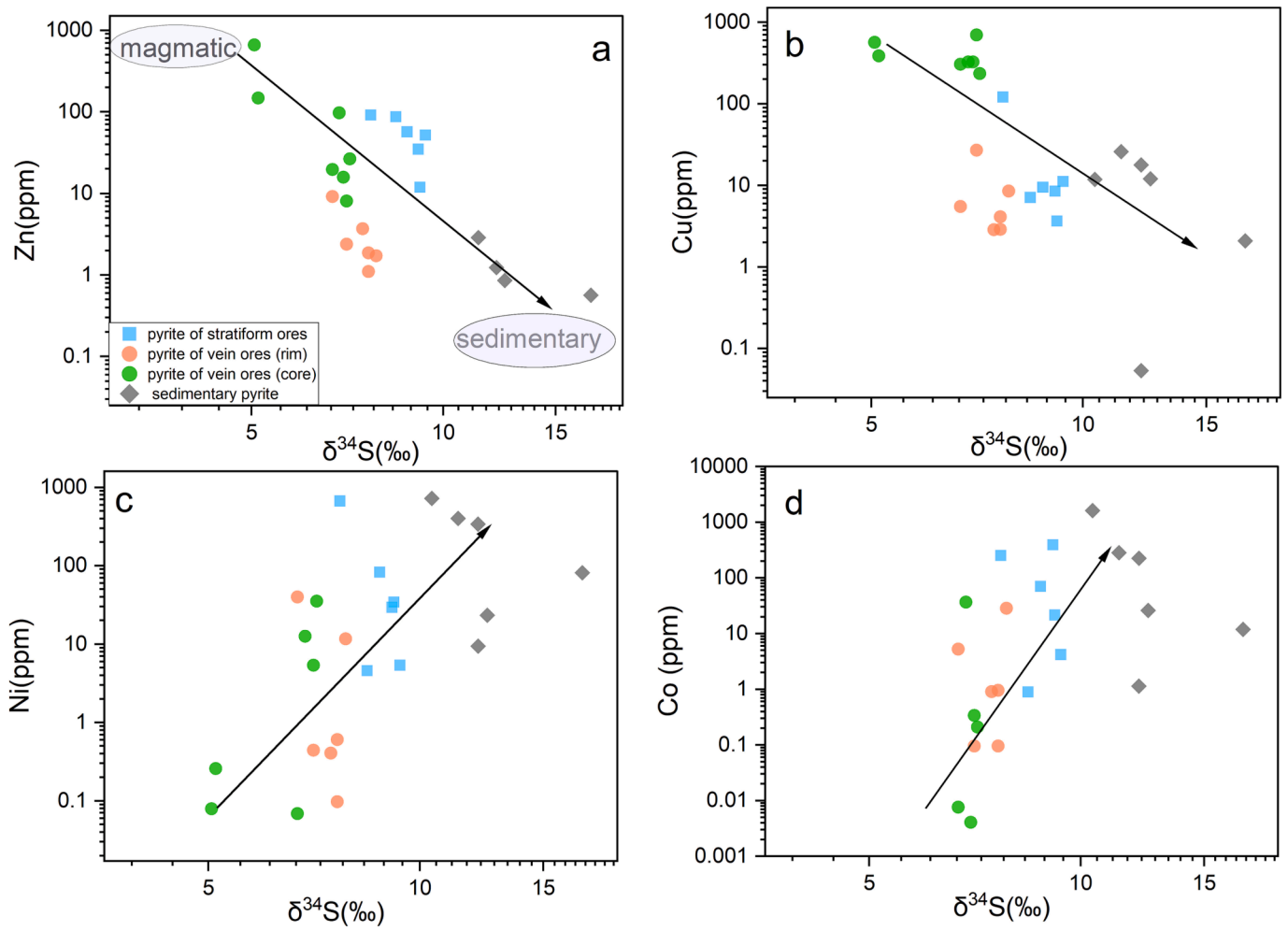

Fig. 11. Correlation between $\delta^{34}S$ values and Cu, Zn, Co, Ni concentrations of pyrites from different types of ores in the Qingchengzi ore district.

original minerals (Py0) as metalliferous fluids circulated through unconsolidated sediments during the sedimentation or early diagenesis (Kelley et al., 2004; Leach et al., 2005). Therefore, other than abundant Co, Ni, the fluid was fertile in metals such as Zn, As, Mn, V, as evidenced by higher Zn, As, Mn, V concentrations of Py1a compared to those of Py0 and the commence of sphalerite (Sp1a) deposition.

The volcanic-sedimentary sequence of the Liaohe Group was affected by regional metamorphism and deformation at 1.93–1.85 Ga. The sequence was transformed to interbedded units of mica schist and marble during greenschist- to lower amphibolite-facies metamorphism, which now host the majority of Pb-Zn orebodies in the Qingchengzi ore district. The mica schist is rich in metals such as Co, Ni, Cr, V, Cu and Zn (Supplementary Table 6), representing an important potential source of metals. The regional metamorphism induced remobilization of many trace elements in early formed sulfides, leading to the loss of most trace elements in Py1b and Sp1b. Cobalt, Ni, Cu, As and Au were expelled from the Py1b, and Cu, Cd, In, Ag and Sb were lost from the Sp1b. This process was likely facilitated by recrystallization and/or metamorphic growth or intra-grain diffusion, which remobilized elements from the crystal lattice of sulfide minerals. On the contrary, Mn of both Py1b and Sp1b are enriched, which reflects a great availability of Mn to be partitioned into sphalerite and pyrite due to the replacement of carbonate wall rock during metamorphism.

In the Mesozoic, there were several episodes of magmatic activities developed in the ore district, forming the Late Triassic, Jurassic, and Early Cretaceous magmatic intrusions reported (Duan et al., 2012; Sun et al., 2020a). Sulfide trace element mapping suggests at least two pulses of magmatic exsolved fluids are responsible for the formation of stage-II sulfides. Combined with previous geochronology data, the early pulse of fluid forming the core of Py2 is derived from the late Triassic magmatic event and is enriched in Cu and Zn. The later pulse of fluid formed the rim of Py2 is Jurassic or Early Cretaceous age, and enriched in Au and As, which is reflected in for the formation of several gold deposits within the ore district. Besides, fluid-rock interaction plays an important role during the second metallogenic event. When magmatic fluids migrate through the wall rocks, the hydrothermal fluids leached S along with Cu, Zn, Co, Ni, V metals from mica schist from the Dashiqiao and Gaixian Formations.

7. Conclusions

(1) The Pb-Zn deposits in the Qingchengzi ore district are the result of multi-stage mineralization, including a Paleoproterozoic sedimentary-metamorphic stage and a Mesozoic magmatic-hydrothermal stage. The Mesozoic stage is further characterized by two episodes of magmatic-hydrothermal mineralization in the Triassic and Jurassic/Cretaceous, respectively.

(2) During the regional metamorphism, trace elements such as Co, Ni, Cu, As and Au were remobilized from pyrite, and Cu, Cd, In, Ag and Sb were remobilized from sphalerite. This process was facilitated by recrystallization and/or metamorphic growth.

(3) Stage-I pyrite formed in a SEDEX setting, showing high Co, Ni, Zn, Mn, V contents which implies a reducing environment. The pyrite and sphalerite formed in the magmatic-hydrothermal stage

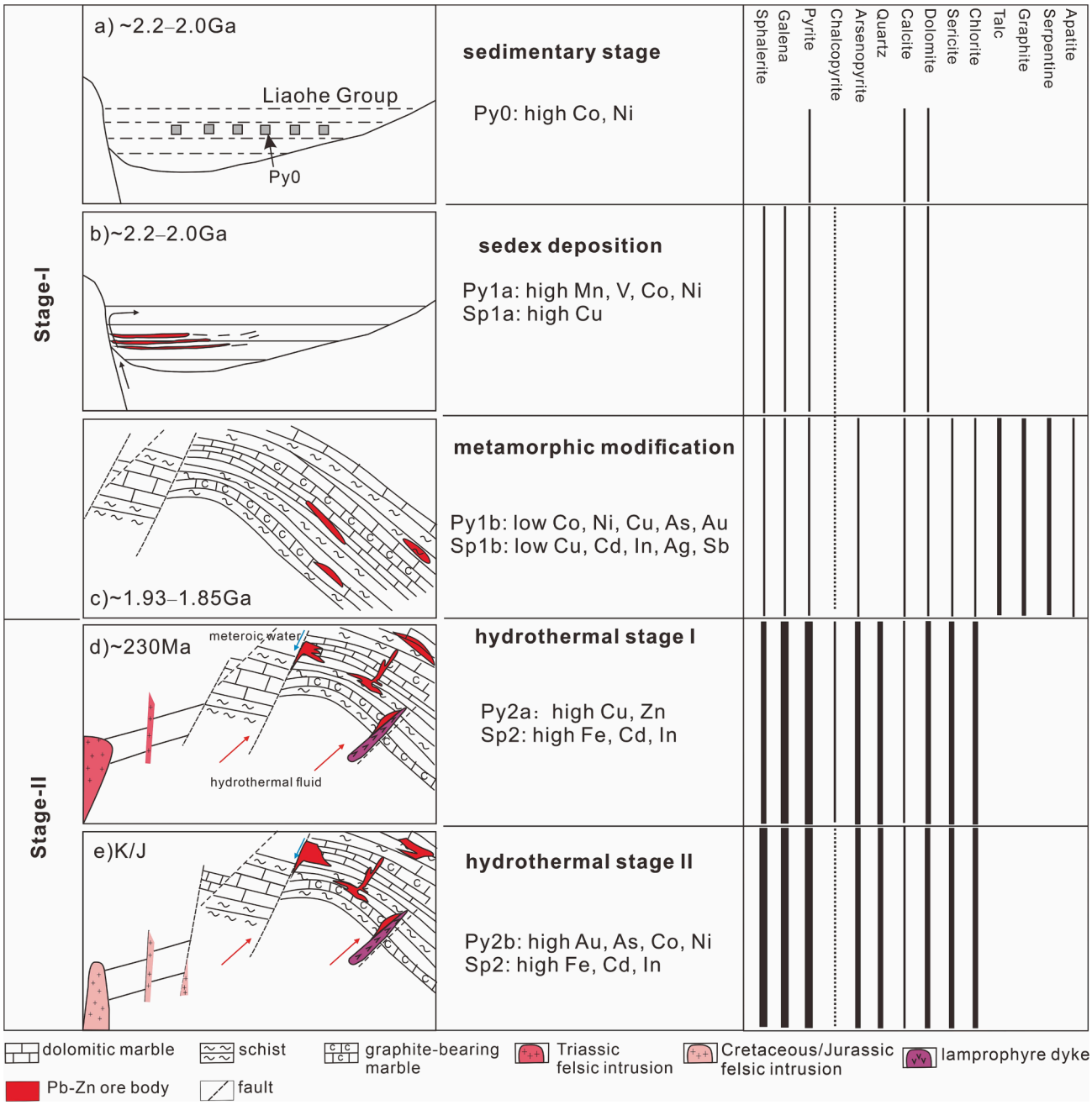

Fig. 12. Schematic figure of ore-forming processes and paragenetic sequences. a) Sedimentary stage at 2.2–2.0 Ga in which the volcanic-sedimentary sequence of the Liaohe Group was deposited; b)SEDEX deposit at 2.2–2.0 Ga in which the Py1a, Sp1a and carbonate minerals were deposited as laminated ores; c) Metamorphic modification at 1.93–1.85 Ga in which the strata as well as primary ores underwent greenschist to lower amphibolite-facies metamorphism. Sulfides were deformed and recrystallized which induced remobilization of metals and loss of Co, Ni, Cu, As, Au of pyrite and Cu, Cd, In of sphalerite; d) Mesozoic hydrothermal stage at ~230 Ma, in which the Cu, Zn enriched magmatic hydrothermal fluid leached S and Cu, Zn, Co, Ni from Liaohe Group and modified the sedmentary-metamorphic stage orebodies and formed Pb-Zn and Pb ore bodies; e) Mesozoic hydrothermal stage at Early Cretaceous or Jurassic, in which Au and As enriched fluids interacted with the Liaohe Group, and overprinted previous mineralization and formed Pb-Zn as well as Au-Ag ore bodies in the district.

(Stage-II) are more enriched in Cu, Ag, Au, As, Sb, Pb, Ga and In compared to stage-I sulfides. The Py2 shows a multigenerational texture, featured with a Cu and Zn enriched core and an overgrowth rim enriched in Au, As, Co and Ni. The compositionally distinct core and rim probably suggests that two episodes of magmatic-hydrothermal fluids were involved in the formation of stage-II sulfides. The Au, Cu and Zn of stage-II mineralization might be predominantly contributed by magmatic fluids, but the Co and Ni might mainly be added by leaching from *meta*-sedimentary rocks.

(4) During the sedimentary-metamorphic mineralization, sulfur was mainly derived from seawater sulfate reduction and the metals from the *meta*-volcanic-sedimentary wall rocks. At the magmatic-hydrothermal stage, magma and wall rocks both contributed sulfur and metals. When fluid-rock interaction proceeded along with the upward migration of magmatic-hydrothermal fluids, the ore-forming fluids leached sulfur along with Cu, Zn, Co, Ni and V metals from the wall rocks of the mica schist of the Dashiqiao and Gaixian formations.

Declaration of competing interest

The authors declare that they have no known competing financial interests or personal relationships that could have appeared to influence the work reported in this paper.

Data availability

Data will be made available on request.

Acknowledgements

This study was financially supported by the National Nature Science Foundation of China (41602068) and National Key Research and Development Program of China (2021YFC2900300 and 2016YFC0600108). We thank Bin Li from the Qingchengzi Mining Ltd for the field assistance, Huan Wang for apatite U-Pb dating analyais, and Kaiyun Chen for S isotope analysis. We are grateful to Prof. Thomas Ulrich for the help of trace element analysis and valuable advices to revise the article. We appreciate two anonymous reviewers for their constructive suggestions, which significantly improved the paper.

Appendix A. Supplementary data

Supplementary data to this article can be found online at https://doi.org/10.1016/j.oregeorev.2023.105829.

References

Andersen, T., 2002. Correction of common lead in U−Pb analyses that do not report 204Pb. Chem. Geol. 192, 50–79.
Berner, Z.A., Puchelt, H., Nöltner, T., Kramar, U.T.Z., 2012. Pyrite geochemistry in the Toarcian Posidonia Shale of south-west Germany: Evidence for contrasting trace-element patterns of diagenetic and syngenetic pyrites. Sedimentology 60, 548–573.
Bodon, S.B., 1998. Paragenetic relationships and their implications for ore genesis at the Cannington. Econ Geol. 93, 1463–1488.
Canfield, D.E., Raiswell, R., 1999. The evolution of the sulfur cycle. Am. J. Sci. 299, 697–723.
Chen, L., Chen, K., Bao, Z., Liang, P., Sun, T., Yuan, H., 2017. Preparation of standards for in situ sulfur isotope measurement in sulfides using femtosecond laser ablation MC-ICP-MS. J. Anal. At. Spectrom. 32, 107–116.
Chew, D.M., Petrus, J.A., Kamber, B.S., 2014. U-Pb LA-ICPMS dating using accessory mineral standards with variable common Pb. Chem. Geol. 363, 185–199.
Cook, N.J., Ciobanu, C.L., Pring, A., Skinner, W., Shimizu, M., Danyushevsky, L., SainiEidukat, B., Melcher, F., 2009. Trace and minor elements in sphalerite: A LA-ICPMS study. Geochim. Cosmochim. Acta 73 (16), 4761–4791.
Cugerone, A., Cenki-Tok, B., Muñoz, M., Kouzmanov, K., Oliot, E., Motto-Ros, V., Goff, E. L., 2021. Behavior of critical metals in metamorphosed Pb-Zn ore deposits: example from the Pyrenean Axial Zone. Miner Deposita 56, 685–705.
Deditius, A.P., Utsunomiya, S., Renock, D., Ewing, R.C., Ramana, C.V., Becker, U., Kesler, S.E., 2008. A proposed new type of arsenian pyrite: Composition, nanostructure and geological significance. Geochim. Cosmochim. Acta 72, 2919–2933.
Dong, A.G., Zhu, X.K., Li, S.Z., Kendall, B., Wang, Y., Gao, Z.F., 2016. Genesis of a giant Paleoproterozoic strata-bound magnesite deposit: Constraints from Mg isotopes. Precambr. Res. 281, 673–683.
Dong, A.G., Zhu, X.K., Li, Z.H., Kendall, B., Li, S.Z., Wang, Y., Tang, C., 2017. A multi-isotope approach towards constraining the origin of large-scale Paleoproterozoic B-(Fe) mineralization in NE China. Precambr. Res. 292, 115–129.
Duan, X.X., 2015. Integrated Research on Metallogenic Characteristics and Ore Genesis of Qingchengzi Polymetallic Ore Field, Liaoning Province (PhD thesis). Chin. Acad. Sci. 1–194 in Chinese with English abstract.
Duan, X.X., Zeng, Q.D., Yang, J.H., Liu, J.M., Wang, Y.B., Zhou, L.L., 2014. Geochronology, geochemistry and Hf isotope of Late Triassic magmatic rocks of Qingchengzi district in Liaodong peninsula, Northeast China. J. Asian Earth Sci. 91, 107–124.
Duan, X.X., Liu, J.M., Wang, Y.B., Zhou, L.L., Li, Y.G., Li, B., Zhang, Z., Zhang, Z.L., 2012. Geochronology, geochemistry and geological significance of Late Triassic magmatism in Qingchengzi orefield, Liaoning. Acta Petrologica Sinica 28 (2), 595–606 in Chinese with English abstract.
Duan, X.X., Zeng, Q.D., Wang, Y.B., Zhou, L.L., Chen, B., 2017. Genesis of the Pb- Zn deposits of the Qingchengzi ore field, eastern Liaoning, China: constraints from carbonate LA- ICPMS trace element analysis and C-O–S–Pb isotopes. Ore Geol. Rev. 89, 752–771.
Gadd, M.G., Layton-Matthews, D., Peter, J.M., Paradis, S.J., 2016. The world-class Howard's Pass SEDEX Zn-Pb district, Selwyn Basin, Yukon. Part I: trace element compositions of pyrite record input of hydrothermal, diagenetic, and metamorphic fluids to mineralization. Miner Deposita 51, 319–342.
Goldhaber, M.B., Kaplan, I.R., 1975. Controls and consequences of sulfate reduction rates in recent marine sediments. Soil Sci. 119, 42–55.
Gregory, D.D., Cracknell, M.J., Large, R.R., McGoldrick, P., Kuhn, S., Maslennikov, V.V., Baker, M.J., Fox, N., Belousov, I., Figueroa, M.C., Steadman, J.A., Fabris, A.J., Lyons, T.W., 2019. Distinguishing ore deposit type and barren sedimentary pyrite using laser ablation-inductively coupled plasma-mass spectrometry trace element data and statistical analysis of large data sets. Econ. Geol. 114, 771–786.
Harlov, D.E., Meighan, C.J., Kerr, I.D., Samson, I.M., 2016. Mineralogy, chemistry and fluid-aided evolution of the Pea Ridge Fe Oxide-(Y plus REE) deposit, southeast Missouri. USA. Econ. Geol. 111, 1963–1984.
Hoefs, J., 2009. Stable Isotope Geochemistry, sixth ed. Springer, Berlin, Heidelberg.
Hoskin, P.W.O., Schaltegger, U., 2003. The composition of zircon and igneous and metamorphic petrogenesis. Rev. Mineral. Geochem. 53, 27–62.
Huerta-Diaz, M.A., Morse, J.W., 1992. Pyritization of trace metals in anoxic marine sediments. Geochim. Cosmochim. Acta 56, 2681–2702.
Jiang, S.Y., Wei, J.Y., 1989. Geochemistry of the Qingchengzi lead–zinc deposit. Miner. Deposita 8, 20–28 in Chinese with English abstract.
Keith, M., Haase, K.M., Schwarz-Schampera, U., Klemd, R., Petersen, S., Bach, W., 2014. Effects of temperature, sulfur, and oxygen fugacity on the composition of sphalerite from submarine hydrothermal vents. Geology 42, 699–702.
Kelley, K.D., Leach, D.L., Johnson, C.A., Clark, J.L., Fayek, M., Slack, J.F., Anderson, V. M., Ayuso, R.A., Ridley, W.I., 2004. Textural, compositional, and sulfur isotope variations of sulfide minerals in the red dog Zn-Pb-Ag deposits, brooks range, Alaska: implications for ore formation. Econ. Geol. 99, 1509–1532.
Large, R.R., Bull, S.W., McGoldrick, P.J., Walters, S., Derrick, G.M., Carr, G.R., 2005. Stratiform and strata-bound Zn-Pb-Ag deposits in Proterozoic sedimentary basins, Northern Australia. Econ. Geol. 100th Anniv. Vol, 931–963.
Large, R.R., Danyushevsky, L., Hollit, C., Maslennikov, V., Meffre, S., Gilbert, S., Bull, S., Scott, R., Emsbo, P., Thomas, H., Singh, B., Foster, J., 2009. Gold and trace element zonation in pyrite using a laser imaging technique: implications for the timing of gold in orogenic and carlin-style sediment-hosted deposits. Econ. Geol. 104, 635–668.
Leach, D., Sangster, D., Kelley, K., Large, R.R., Garven, G., Allen, C., Gutzmer, J., Walters, S., 2005. Sediment-hosted lead-zinc deposits: a global perspective. Econ. Geol. 100, 561–607.
Li, S.Z., Zhao, G.C., Sun, M., Han, Z.Z., Luo, Y., Hao, D.F., Xiao, X.P., 2005. Deformation history of the Paleoproterozoic Liaohe assemblage in the Eastern block of the North China Craton. J. Asian Earth Sci. 24 (5), 659–674.
Li, S.Z., Zhao, G.C., 2007. SHRIMP U-Pb zircon geochronology of the Liaoji granitoids, constraints on the evolution of the Paleoproterozoic Jiao–Liao–Ji belt in the Eastern Block of the North China Craton. Precambr. Res. 158, 1–16.
Liu, S.J., Chen, B., Zheng, J.H., Wu, Y.F., Bao, C., Zhao, G.C., 2022. A metamorphic devolatilization model for the genesis of the Baiyun gold deposit in the North China Craton: A novel Fe-S isotopes perspective. Gondwana Res. 106, 126–141.
Liu, G.X., Deng, Y.F., Yuan, F., Chen, X.J., Yang, B., 2021. Rb–Sr dating and S-Sr-Nd isotopic constraints on the genesis of the Hehuashan Pb–Zn deposit in the Middle Lower Yangtze River Metallogenic belt. China. Solid Earth Sci. 6, 57–69.
Liu, Y.S., Hu, Z.C., Gao, S., Günther, D., Xu, J., Gao, C.G., Chen, H.L., 2008. In situ analysis of major and trace elements of anhydrous minerals by LA-ICP-MS without applying an internal standard. Chem Geol. 257, 34–43.
Liu, Z.Y., Xu, X.C., Tian, Y.C., Yang, D.J., Jiang, Y.Z., Tian, S.H., Wei, M., 2007. Relationship between sedimentation–exhalation ore–forming process and gold–silver polymetallic mineralization in Qingchengzi area, Liaoning Province. Miner. Deposita 26, 563–571 in Chinese with English abstract.
Lockington, J.A., Cook, N.J., Ciobanu, C.L., 2014. Trace and minor elements in sphalerite from metamorphosed sulphide deposits. Mineral Petrol. 108, 873–890.
Luo, Y., Sun, M., Zhao, G.C., Li, S.Z., Ayers, J.C., Xia, X., Zhang, J., 2008. A comparison of U-Pb and Hf isotopic compositions of detrital zircons from the North and South Liaohe Groups, constraints on the evolution of the Jiao–Liao–Ji Belt, North China Craton. Precambr. Res. 163, 279–306.
Lusk, J., Scott, S.D., Ford, C.E., 1993. Phase relations in the Fe-Zn-S system to 5 Kbars and temperatures between 325° and 150° C. Econ. Geol. 88, 1880–1903.
Ma, Y.B., Du, X.H., Zhang, Z.J., Xing, S.W., Zou, Y.F., Li, B., Yang, X.Q., Wang, Y., 2013. REE geochemical characteristics of Qingchengzi stratiform/veined Pb–Zn ore district. Miner. Deposita 32 (6), 1236–1248 in Chinese with English abstract.
Ma, Y.B., Bagas, L., Xing, S.W., Zhang, S.T., Wang, R.J., Li, N., Zhang, Z.J., Zou, Y.F., Yang, X.Q., Wang, Y., Zhang, Y., 2016. Genesis of the stratiform Zhenzigou Pb-Zn deposit in the North China Craton: Rb-Sr and C-O-S-Pb isotope constraints. Ore Geol. Rev. 79, 88–104.
Marshall, B., Gilligan, L.B., 1993. Remobilization, syn-tectonic processes and massive sulphide deposits. Ore Geol. Rev. 8, 39–64.
Maslennikov, V.V., Maslennikova, S.P., Large, R.R., Danyushevsky, L.V., 2009. Study of trace element zonation in vent chimneys from the Silurian Yaman-Kasy volcanic-hosted massive sulfide deposit (Southern Urals, Russia) using laser ablation-inductively coupled plasma mass spectrometry (LA-ICPMS). Econ. Geol. 104, 1111–1141.
Meng, Y.M., Hu, R.Z., Huang, X.W., Gao, J.F., Qi, L., Lyn, C., 2018. The relationship between stratabound Pb-Zn-Ag and porphyry-skarn Mo mineralization in the Laochang deposit, southwestern China: Constraints from pyrite Re-Os isotope, sulfur isotope, and trace element data. J. Geochem. Explor. 194, 218–238.
Mishra, B., Bernhardt, H.J., 2009. Metamorphism, graphite crystallinity, and sulfide anatexis of the Rampura-Agucha massive sulfide deposit, northwestern India. Miner. Deposita 44, 183–204.

Ohmoto, H., 1972. Systematics of sulfur and carbon isotopes in hydrothermal ore-deposits. Econ. Geol. 67, 551–578.
Orr, W.L., 1974. Changes in sulfur content and isotopic ratios of sulfur during petroleum maturation; study of big horn basin Paleozoic oils. AAPG Bull. 58, 2295–2318.
Paton, C., Hellstrom, J., Paul, B., Woodhead, J., Hergt, J., 2011. Iolite: Freeware for the visualization and processing of mass spectrometric data. J. Anal. At. Spectrom. 26, 2508–2518.
Ramdohr, P., 1969. The ore minerals and their intergrowths, 3rd ed. Pergamon Press, New York.
Reiser, F.K.M., Rosa, D.R.N., Pinto, Ã.M.M., Carvalho, J.R.S., Matos, J.X., Guimaraes, F. M.G., Alves, L.C., de Oliveira, D.P.S., 2011. Mineralogy and geochemistry of tin- and germanium-bearing copper ore, Barrigao re-mobilized vein deposit, Iberian Pyrite Belt, Portugal. Int. Geol. Rev. 53, 1212–1238.
Song, J.C., 2010. Minerogenetic series and ore–forming processes of metal deposits in the Liaodong Rift. Northeastern University, Liaoning, pp. 42–48. PhD thesis (in Chinese with English abstract).
Song, Y.H., Yang, F.C., Yan, G.L., Wei, M.H., Shi, S.S., 2016. SHRIMP U-Pb ages and Hf isotopic compositions of Paleoproterozoic granites from the eastern part of Liaoning province and their tectonic significance. Acta Geol. Sin. 90, 2620–2636 in Chinese with English abstract.
Sun, G.T., Zeng, Q., Zhou, L.L., Wang, Y.B., Chen, P.W., 2020a. Trace element contents and in situ sulfur isotope analyses of pyrite in the Baiyun gold deposit, NE China: implication for the genesis of intrusion-related gold deposits. Ore Geol. Rev. 118, 103330.
Sun, G.T., Zeng, Q.D., Wang, Y.B., Li, B., Chen, P.W., 2020b. Geochronology and geochemistry of Mesozoic dykes in the Qingchengzi ore field, Liaoning Province, China: magmatic evolution and implications for ore genesis. Geol. J. 55, 5745–5763.
Sun, G.T., Zeng, Q.D., Zhou, L.L., Hollis, S.P., Zhou, J.X., Chen, K.Y., 2022. Mechanisms for invisible gold enrichment in the Liaodong Peninsula, NE China: in situ evidence from the Xiaotongjiapuzi deposit. Gondwana Res. 103, 276–296.
Sun, G.T., Zeng, Q.D., Zhou, J.X., 2023. Jurassic Au–Ag mineralization of the Linjiasandaogou deposit in the Liaodong Peninsula, northeast China: Evidence from apatite U-Pb dating and the in situ geochemistry of sulfides. J. Geochem. Explor. 251, 107242.
Tam, P.Y., Zhao, G.C., Liu, F.L., Zhou, X.W., Sun, M., Li, S.Z., 2011. Timing of meta–morphism in the Paleoproterozoic Jiao–Liao–Ji Belt, new SHRIMP U-Pb zircondating of granulites, gneisses and marbles of the Jiaobei massif in the NorthChina Craton. Gondwana Res 19, 150–162.
Thomas, H.V., Large, R.R., Bull, S.W., Maslennikov, V., Berry, R.F., Fraser, R., Froud, S., Moye, R., 2011. Pyrite and pyrrhotite textures and composition in sediments, laminated quartz veins, and reefs at Bendigo Gold Mine, Australia: insights for ore genesis. Econ. Geol. 106, 1–31.
Tian, Z., Liu, F., Windley, B.F., Liu, P., Wang, F., Liu, C., 2017. Polyphase structural deformation of low- to medium-grade metamorphic rocks of the Liaohe group in the Jiao-Liao-Ji Orogenic Belt, North China Craton: correlations with tectonic evolution. Precambr. Res. 303, 641–659.
Tiu, G., Jansson, N., Wanhainen, C., Ghorbani, Y., Lilja, L., 2021. Ore mineralogy and trace element (re)distribution at the metamorphosed Lappberget Zn-Pb-Ag-(Cu-Au) deposit, Garpenberg. Sweden. Ore Geol. Rev. 135, 104223.
Wagner, T., Klemd, R., Wenzel, T., Mattsson, B., 2007. Gold upgrading in metamorphosed massive sulfide ore deposits: direct evidence from laser-ablation-inductively coupled plasma-mass spectrometry analysis of invisible gold. Geology 35, 775–778.
Wan, Y.S., Song, B., Liu, D.Y., Wilde, S.A., Wu, J.S., Shi, Y.R., Yin, X.Y., Zhou, H.Y., 2006. SHRIMP UPb zircon geochronology of Paleoproterozoic metasedimentary rocks in the North China Craton, Evidence for a major Late Paleoproterozoic tectonothermal event. Precambr. Res. 149, 249–271.
Wang, Y.Z., Wang, F., Shi, W.B., Yang, L.K., Wu, L., 2020. Timing and Processes of Ore Formation in the Qingchengzi Polymetallic Orefield, Northeast China: Evidence from 40Ar/39Ar Geochronology. Acta Geol. Sin. (English Edition) 94, 789–800.
Wei, B., Wang, C.Y., Wang, Z.C., Cheng, H., Xia, X.P., Tan, W., 2021. Mantle-derived gold scavenged by bismuth-(tellurium)-rich melts: Evidence from the mesozoic wulong gold deposit in the north china craton. Ore Geol. Rev. 131, 104047.
Wu, F.Y., Yang, J.H., Liu, X.M., 2005. Geochronological framework of the Mesozoic granitic magmatism in the Liaodong Peninsula. Northeast China. Geol. J. China Univ. 11, 305–317 in Chinese with English abstract.
Xie, L.W., Zhang, Y.B., Zhang, H.H., Sun, J.F., Wu, F.Y., 2008. In-situ simultaneous determination of trace elements, U−Pb and Lu−Hf isotopes in zircon and baddeleyite. Chinese Sci. Bull. 53, 1565–1573 in Chinese.
Xu, L., Yang, J.H., Zeng, Q.D., Xie, L.W., Zhu, Y.S., Li, R., Li, B., 2020. Pyrite Rb-Sr, Sm-Nd and Fe isotopic constraints on the age and genesis of Pb-Zn deposits in Qingchengzi, northeastern China. Ore Geol Rev. 103324.
Yang, Z.J., Zhang, J., Liu, C.C., Yang, X.Y., Wang, C.H., Jiang, C.Y., 2015. Geochemistry and genesis of the metamorphic rocks of Liaohe Group in Huangqi area, Laioning Province. Geol. Resour. 24, 353–361 in Chinese with English abstract.
Yu, G., Chen, J.F., Xue, C.J., 2009. Geochronological framework and Pb, Sr isotope geochemistry of the Qingchengzi PbZnAgAu ore field, Northeastern China. Ore Geol. Rev. 35, 367–382.
Yu, P.P., Zheng, Y., Wang, C.M., 2020. Trace elemental and sulfur-lead isotopic variations in metamorphosed volcanogenic massive sulfide (VMS) mineralization systems: An example from the Keketale Pb-Zn(-Ag) deposit, NW China. Ore Geol. Rev. 125, 103685.
Zeng, Q.D., Chen, P.Y., Yang, J.H., Sun, G.T., Yu, B., Wang, Y.B., Chen, P.W., 2019. The metallogenic characteristics and exploring ore potential of the gold deposits in eastern Liaoning Province. Acta Petrol. Sin. 35 (7), 1939–1963 in Chinese with English abstract.
Zhang, Q.S., 1984. Early Precambrian Geology and Metallogenesis in China. People's Publishing House of Jilin, Changchun, pp. 65–248 in Chinese.
Zheng, Y., Wang, Y.J., Chen, H.Y., Lin, Z.W., Hou, W.S., Li, D.F., 2016. Micro-textural and fluid inclusion data constraints on metallic remobilization of the Ashele VMS Cu-Zn deposit, Altay, NW China. J. Geochem. Explor. 171, 113–123.
Zhou, L.L., Zeng, Q.D., Sun, G.T., Duan, X.X., Bonnetti, C., Riegler, T., Long, D.G.F., Kamber, B., 2019. Laser Ablation-inductively coupled plasma mass spectrometry (LA-ICPMS) elemental mapping and its applications in ore geology. Acta Petrol. Sin. 35 (7), 1964–1978 in Chinese with English abstract.
Zhou, L.L., Zeng, Q.D., Liu, J.M., Duan, X.X., Sun, G.T., Wang, Y.B., Chen, P.W., 2020. Tracing mineralization history from the compositional textures of sulfide association: A case study of the Zhenzigou stratiform Zn-Pb deposit, NE China. Ore Geol. Rev. 126, 103792.
Zhu, J.J., Liu, F.L., Wang, F., Xu, W.T., Liu, F.X., Shi, C., 2021. Carbon isotope and geochemical characteristics of the Paleoproterozoic graphite deposits in the Jiao-Liao-Ji belt, North China Craton: Implications for genesis and depositional environment. Precambr. Res. 362, 106320.